

NO-A191 537

TRANSIENT PARTICLE DEPOSITION IN A BOUNDARY LAYER OF
IMPULSIVE FLOW OVER A FLAT PLATE(U) WASHINGTON STATE
UNIV PULLMAN DEPT OF MECHANICAL ENGINEERING.

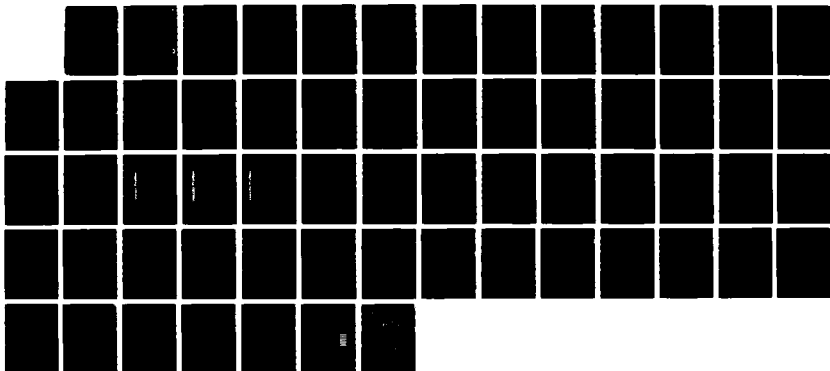
1/1

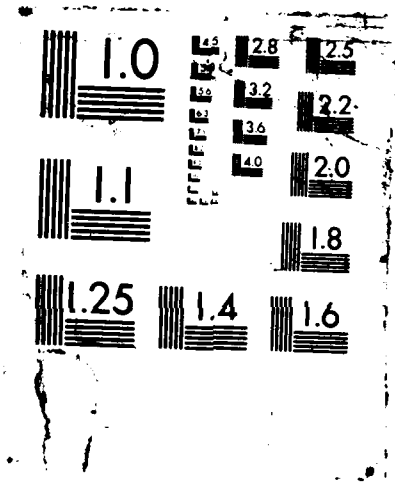
UNCLASSIFIED

J N CHUNG NOV 87 BRL-CR-589

F/G 28/4

NL





DTIC FILE COPY

ADP 301028

AD (4)

AD-A191 537

CONTRACT REPORT BRL-CR-589

TRANSIENT PARTICLE DEPOSITION IN A
BOUNDARY LAYER OF IMPULSIVE FLOW
OVER A FLAT PLATE

WASHINGTON STATE UNIVERSITY
DEPARTMENT OF MECHANICAL ENGINEERING
PULLMAN, WASHINGTON 99164-2920

NOVEMBER 1987

DTIC
SELECTED
FEB 19 1988
S E D

APPROVED FOR PUBLIC RELEASE; DISTRIBUTION UNLIMITED.

US ARMY BALLISTIC RESEARCH LABORATORY
ABERDEEN PROVING GROUND, MARYLAND

88 2 18 02 5

DESTRUCTION NOTICE

Destroy this report when it is no longer needed. DO NOT return it to the originator.

Additional copies of this report may be obtained from the National Technical Information Service, U.S. Department of Commerce, Springfield, VA 22161.

The findings of this report are not to be construed as an official Department of the Army position, unless so designated by other authorized documents.

The use of trade names or manufacturers' names in this report does not constitute indorsement of any commercial product.

UNCLASSIFIED

SECURITY CLASSIFICATION OF THIS PAGE

REPORT DOCUMENTATION PAGE				Form Approved OMB No 0704-0188 Exp. Date Jun 30, 1986	
1a. REPORT SECURITY CLASSIFICATION Unclassified		1b. RESTRICTIVE MARKINGS			
2a. SECURITY CLASSIFICATION AUTHORITY		3. DISTRIBUTION / AVAILABILITY OF REPORT			
2b. DECLASSIFICATION / DOWNGRADING SCHEDULE					
4. PERFORMING ORGANIZATION REPORT NUMBER(S)		5. MONITORING ORGANIZATION REPORT NUMBER(S) BRL-CR-589			
6a. NAME OF PERFORMING ORGANIZATION Washington State University		6b. OFFICE SYMBOL (if applicable)	7a. NAME OF MONITORING ORGANIZATION US Army Ballistic Research Laboratory		
6c. ADDRESS (City, State, and ZIP Code) Department of Mechanical Engineering Pullman, Washington 99164-2920		7b. ADDRESS (City, State, and ZIP Code) ATTN: SLCBR-IB-A Aberdeen Proving Ground, Maryland 21005-5066			
8a. NAME OF FUNDING / SPONSORING ORGANIZATION		8b. OFFICE SYMBOL (if applicable)	9. PROCUREMENT INSTRUMENT IDENTIFICATION NUMBER		
8c. ADDRESS (City, State, and ZIP Code)		10. SOURCE OF FUNDING NUMBERS			
		PROGRAM ELEMENT NO. 61102A	PROJECT NO. 1L161102AH	TASK NO. 3	WORK UNIT ACCESSION NO. 00
11. TITLE (Include Security Classification) Transient Particle Deposition in a Boundary Layer of Impulsive Flow Over a Flat Plate					
12. PERSONAL AUTHOR(S) Jacob N. Chung					
13a. TYPE OF REPORT Contract Report		13b. TIME COVERED FROM Jul 85 TO Aug 85	14. DATE OF REPORT (Year, Month, Day)		15. PAGE COUNT
16. SUPPLEMENTARY NOTATION					
17. COSATI CODES			18. SUBJECT TERMS (Continue on reverse if necessary and identify by block number)		
FIELD	GROUP	SUB-GROUP	Particle deposition, discrete vortex method, boundary layer		
19	01				
21	02				
19. ABSTRACT (Continue on reverse if necessary and identify by block number) <p>The transport and deposition of fine particles in a boundary layer of impulsive flow over a flat plate have been examined by numerical methods. The transient impulsive flow over a flat plate is solved by a vortex sheet method and the particle transport equation is numerically integrated by the Strongly Implicit Procedure. The transient solutions are preliminary because refinement of the computer program is needed. Some trends and interesting features may be drawn from the results.</p>					
20. DISTRIBUTION / AVAILABILITY OF ABSTRACT <input checked="" type="checkbox"/> UNCLASSIFIED/UNLIMITED <input checked="" type="checkbox"/> SAME AS RPT <input checked="" type="checkbox"/> DTIC USERS			21. ABSTRACT SECURITY CLASSIFICATION Unclassified		
22a. NAME OF RESPONSIBLE INDIVIDUAL Kurt D. Fickie			22b. TELEPHONE (Include Area Code) (301)278-6106		22c. OFFICE SYMBOL SLCBR-IB-A

TABLE OF CONTENTS

	Page
LIST OF ILLUSTRATIONS.....	5
INTRODUCTION.....	7
MATHEMATICAL MODEL.....	9
A. Flow Field-Impulsive Flow over a Flat Plate.....	9
B. Particle Transport.....	17
VERIFICATION OF THE COMPUTATIONAL SCHEMES.....	27
A. Flow Field Calculations.....	27
B. Particle Transport Computations.....	33
B.1 Comparision with Exact Solutions.....	33
B.2 Steady State Comparision.....	35
SOLUTION PROCEDURE.....	36
RESULTS AND DISCUSSION.....	36
CONCLUSIONS.....	45
RECOMMENDATIONS.....	50
SUMMARY.....	51
ACKNOWLEDGEMENT.....	51
REFERENCES.....	52

Accession For	
NTIS GRA&I	<input checked="" type="checkbox"/>
DTIC TAB	<input type="checkbox"/>
Unannounced	<input type="checkbox"/>
Justification	
By _____	
Distribution/ _____	
Availability Codes	
Dist	Avail and/or Special
A-1	



LIST OF ILLUSTRATIONS

Figure	Page
1 The Schematic of the Flow System.....	10
2 Particle Transport Mechanism at the Boundary.....	20
3 The Grid System for Transport Equation.....	24
4 The Drag Coefficeint of Impulsive Boundary Layer.....	29
5 Typical Vortex Sheet Positions in Boundary Layer.....	30
6 Typical Instantaneous Velocity Profiles.....	31
7 Comparision of Predicted Velocity Profiles with that of the Blasius Solution.....	32
8 Instantaneous Deposition Rates for Various Reynolds Numbers.....	40
9 Time-Averaged Deposition Rates for Various Reynolds Numbers.....	41
10 Accumulated Particle Depositions for Various Reynolds Numbers.....	43
11 Time-Averaged Deposition Rates for Various Sc Numbers.....	44
12 Time-Averaged Deposition Rates for Various Tr Numbers.....	46
13 Steady State Deposition Rates as a Function of Reynolds Numbers.....	47
14 Steady State Deposition Rates as a Function of Schmidt Numbers.....	48
15 Steady State Deposition Rates as a Function of Transport Numbers.....	49

INTRODUCTION

The transport and deposition of entrained particles from the flow stream onto the walls which contain the flow have been under investigation for the past thirty years. Because of the complicated nature of the problem, research work has been limited to rather simplified conditions. In general, the transport mechanism is strongly dependent on the particle size and the characteristics of the flow field. Among the early investigations, Friedlander and Johnstone¹ developed a theory for relatively large particles ($>1\mu$) and Lin et al.² investigated the molecular-size (dissolved) particles. For small particles, the transport is dominated by the Brownian diffusion while for larger particles, the particle's momentum has to be included in addition to molecular diffusion. To include the inertia effect of the larger particles, it is suggested that they only need to diffuse to within one stopping distance from the wall; from that point on, the particles will coast to the wall by virtue of their momentum. Since the stopping distance could be appreciable compared to their sizes, the deposition rates are far in excess of those resulting from pure diffusion. For small particles, however, the stopping distance is negligibly small such that diffusion dominates all the way to the wall. Beal³ developed a model that combines both concepts of small and large particles discussed above. His method predicts the deposition of particles ranging from molecular size to 10μ in a channel or pipe for steady turbulent flow. Menguturk and Sverdrup⁴ applied Beal's³ method to

¹Friedlander, S.K., and Johnstone, H.F., "Deposition of Suspended Particles from Turbulent Gas Streams," *Industrial and Engineering Chemistry*, 49, 1957.

²Lin, C.S., Moulton, R.W., and Putman, G.L., "Mass Transfer Between Solid Wall and Fluid Streams," *Industrial and Engineering Chemistry*, 45, 1953.

³Beal, S.K., "Departion of Particles in Turbulent Flow on Channel or Pipe Walls," *Nuclear Science and Engineering*, 40, 1970.

⁴Menguturk, M. and Sverdrup, E.F., "A Theory for Fine Particle Deposition in Two-Dimensional Boundary Layer Flows and Application to Gas Turbines," *J. of Engineering for Power*, 104, 69-70, 1982.

the prediction of fine particle deposition in steady two-dimensional boundary layer with application to the gas turbine operation. For even larger particles ($>10\mu$), inertia effects dominate and the approach is to derive the equation of motion for each particle and follow their trajectories (Lagrangian method). Ganic and Rohsenow⁵ investigated the large liquid drop deposition in two-phase pipe flow. The equation of motion for each drop was developed taking into account drag forces, buoyancy forces, gravity forces, lift forces, and reaction forces due to evaporation. The deposition rates predicted by this Lagrangian model help explain the behavior found in measurements of boiling heat transfer with dispersed flow.

As a result of the literature survey, it was found that no published reports deal with the transient aspect of particle transport. The unsteady particle transport is encountered in many short time-frame processes. The deposition rates of particles are usually much higher and some special characteristics may not be predicted by a steady state analysis. In this report, the transport and deposition of particles with diameters ranging between molecular size and 10μ are analyzed for flow impulsively started over a flat plate. The flow stream entraining the fine particles is numerically simulated by the vortex sheet model proposed by Chorin⁶. The transient particle transport equation is solved by the Strongly Implicit Procedure developed by Stone⁷. The objective of this study is to obtain the particle deposition rates as a function of time, particle size and flow conditions.

⁵Ganic, E.N. and Rohsenow, W.M., "On the Mechanism of Liquid Drop Deposition in Two-Phase Dispersed Flow," J. of Heat Transfer, 101, 228-294, 1979.

⁶Chorin, A.J., "Vortex Sheet Approximation of Boundary Layers," J. of Computational Physics, 27, 428-442, 1978.

⁷Stone, H.L., "Iterative Solution of Implicit Approximations of Multidimensional Partial Differential Equations," SIAM J. Numerical Analysis, 5, 530-558, 1968.

MATHEMATICAL MODEL

A. Flow Field - Impulsive Flow over a Flat Plate

A vortex sheet method proposed by Chorin⁶ is adopted for the flow simulation.

The governing equation is the unsteady Navier-Stokes equation in terms of vorticity, and the schematic is shown in Figure 1.

$$\frac{\partial \xi}{\partial t} + (\vec{u} \cdot \nabla) \xi = \nu \frac{\partial^2 \xi}{\partial y^2} \quad (1)$$

$$\xi = - \frac{\partial u}{\partial y} \quad (2)$$

$$\frac{\partial u}{\partial x} + \frac{\partial v}{\partial y} = 0 \quad (3)$$

where ξ is the two-dimensional vorticity scalar, ν is the kinematic viscosity of the fluid. $\vec{u} = (u, v)$ is the velocity vector, u is the velocity component in the x -direction and v is the velocity in the y -direction. It is noted that equations (1), (2), and (3) include the boundary layer approximations.

The initial and boundary conditions are

$$u = u_{\infty}, v = 0, t = 0^+ \quad (4)$$

$$u \rightarrow u_{\infty}, y \rightarrow \infty \text{ and } t > 0 \quad (5)$$

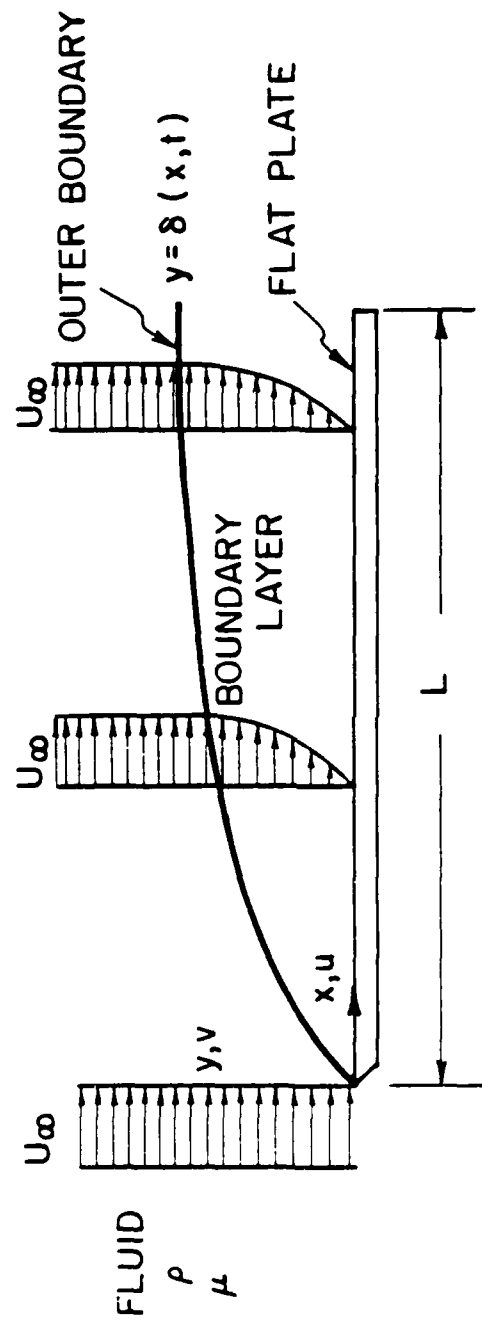


Figure 1. The Schematic of the Flow System

$$u = 0, v = 0, y = 0 \text{ and } t > 0 \quad (6)$$

where u_∞ is the steady free stream velocity.

The governing equation and the initial and boundary conditions may be non-dimensionalized by the following, with L being the length of the plate,

$$\bar{\xi} = \frac{\xi L}{u_\infty}, \bar{u} = u/u_\infty, \bar{v} = v/u_\infty, \bar{x} = x/L, \bar{y} = y/L \text{ and } \bar{t} = tu_\infty/L \quad (7)$$

The dimensionless governing equation and the auxillary conditions then become

$$\frac{\partial \bar{\xi}}{\partial \bar{t}} + \bar{u} \frac{\partial \bar{\xi}}{\partial \bar{x}} + \bar{v} \frac{\partial \bar{\xi}}{\partial \bar{y}} = \frac{1}{Re_L}, \frac{\partial^2 \bar{\xi} L}{\partial \bar{y}^2} Re_L = \frac{v_\infty L}{u} \quad (8)$$

$$\bar{\xi} = - \frac{\partial \bar{u}}{\partial \bar{y}} \quad (9)$$

$$\frac{\partial \bar{u}}{\partial \bar{x}} + \frac{\partial \bar{v}}{\partial \bar{y}} = 0 \quad (10)$$

$$\bar{u} = 1, \bar{v} = 0, \bar{t} = 0^+ \quad (11)$$

$$\bar{u} \rightarrow 1, \bar{y} \rightarrow \infty \text{ and } \bar{t} > 0 \quad (12)$$

$$\bar{u} = 0, \bar{v} = 0, \bar{y} = 0 \text{ and } \bar{t} > 0 \quad (13)$$

The bars will be dropped from this point on.

Only one parameter, Re , results in the dimensionless system. It is well known that the numerical solution becomes more difficult as the Reynolds number increases, and the analytical solution is intractable. Chorin⁸ indicated that the mesh width δ in a finite difference scheme must satisfy the following condition in order to maintain stability.

$$\delta Re = O(1) \quad (14)$$

Therefore for relatively high Reynolds number flow, the number of mesh points required to obtain a solution would be prohibitive. Accordingly, it is of interest to develop a grid-free numerical method. One approach which has been used with considerable success involves simulating the fluid field using discrete vortex elements. The interaction between these vortex elements is then used to model the developing flow field. This method was first used by Chorin⁸ and has since been applied by numerous researchers to various turbulent shear flows with surprising success. These numerical simulations have depicted the existence and interaction of large scale vortex structures in qualitative agreement with flow visualizations. Quantitative results of mean velocity and turbulence intensities have also been in reasonable agreement with experiments. These successes have been especially impressive in view of the fact that, in most cases, the simulation has been restricted to a two-dimensional model.

Chorin⁸ has demonstrated that the vortex method overcomes many difficulties encountered with the finite difference scheme for flows in separated regions or in the wake of an object. Especially for the recirculating turbulent flow, the constant change of flow direction and velocity gradient prevent the grid-system approach from obtaining accurate solutions due to accumulated truncation and round-off errors. The "discrete vortex method" is essentially a numerical simulation of the

⁸Chorin, A.J., "Numerical Study of Slightly Viscous Flows," *J. of Fluid Mechanics*, 57, 785-796, 1973.

process of vorticity generation and dispersal; therefore, it is grid-free. The vorticity in the fluid is grouped into vortex "blobs" and their motion is governed by both the random displacement using computer-generated pseudo-random numbers and mutual interaction effects. The process is time-dependent and all the vortex blobs have to be followed at all time while they are present in the system.

These direct numerical vortex methods require little or no empirical information for computing the flow field and more importantly they give transient instantaneous flow information. This gives them a decided advantage over empirical time average turbulence models.

The vortex sheet model⁶ is an extension of the vortex blob method.⁸ It overcomes both the convergence problem near boundaries and the specific vortex blob structure requirement of the vortex blob method.

The solution of equation (8) is composed of two parts. First the convective motion of the vorticity, i.e., solution of the following equation,

$$\frac{\partial \xi}{\partial t} + u \frac{\partial \xi}{\partial x} + v \frac{\partial \xi}{\partial y} = 0 \quad (15)$$

The above equation corresponds to the inviscid part of the equation (8) or when $Re \rightarrow \infty$.

In the absence of boundaries by partitioning the vorticity ξ into a sum of vortex sheets of vorticity ξ_i ,

$$\xi = \sum_{j=1}^N \xi_j \quad (16)$$

Equation (10) can be integrated to give

$$v(y) = \frac{\partial}{\partial x} \int_0^y u(x, z) dz \quad (17)$$

and equation (9) yields

$$u(x,y) = 1 - \int_y^{\infty} \xi(x,z) dz \quad (18)$$

It is seen that if $\xi(x,z)$ is known, (17) and (18) yield u and v .

Based on (16), consider a collection of N segments S_i of vortex sheets, of intensities ξ_i , $i = 1, \dots, N$. These sheets are segments of straight line such that u on one side of S_i and u on the other side of S_i differ by ξ_i . S_i is parallel to x axis of length h and center at $r_i = (x_i, y_i)$. The motion of each vortex sheet is determined by all other sheets in the flow. If (u_i, v_i) is the velocity of S_i , then according to equation (18)

$$u_i = 1 - \frac{1}{2} \xi_i - \sum_j \xi_j d_j \quad (19)$$

where

$$d_j = 1 - (|x_i - x_j|/h) \quad (20)$$

and the sum Σ is over all S_j such that

$$y_j > y_i \text{ and } |x_i - x_j| < h \quad (21)$$

and the vertical velocity v_i can be approximated from (17) by

$$v_i = (I_1 - I_2)/h \quad (22)$$

$$I_1 = (x_i + h/2)y_i - \sum_{j+} \xi_j d_j^+ y_j^* \quad (23)$$

$$I_2 = (x_i - h/2)y_i - \sum_{j-} \xi_j d_j^- y_j^* \quad (24)$$

where

$$d_j^+ = 1 - |x_i + h/2 - x_j|/h \quad (25)$$

$$d_j^- = 1 - |x_i - h/2 - x_j|/h \quad (26)$$

$$y_j^* = \min(y_i, y_j) \quad (27)$$

The sum \sum_{j+} is over all S_j such that $0 \leq d_j^+ \leq 1$ and the sum \sum_{j-} is over all S_j such that $0 \leq d_j^- \leq 1$.

Once (u_i, v_i) is known, the vortex sheet S_i , located at (x_i^n, y_i^n) at time step n , will move to (x_i^{n+1}, y_i^{n+1}) at time step $n+1$ by the first order accurate finite difference equation

$$x_i^{n+1} = x_i^n + (\Delta t)u_i^n \quad (28)$$

$$y_i^{n+1} = y_i^n + (\Delta t)v_i^n \quad (29)$$

where Δt is the time step size and (u_i^n, v_i^n) is the velocity of S_i at time step n .

The second part of the solution is dealing with the viscous diffusion portion.

$$\frac{\partial \xi}{\partial t} = \frac{1}{\text{Re}} \frac{\partial^2 \xi}{\partial y^2} \quad (30)$$

with initial condition $\xi(0) = \xi(x, y, t=0)$.

A solution of this equation using random walks can be obtained as follows. Distribute over the x - y plane points of masses ξ_j and locations $r_i = (x_i, y_i)$, $i=1, \dots, N$, N large, in such a way that the mass density approximates $\xi(0)$. Then move the points according to the following

$$x_i^{n+1} = x_i^n \quad (31)$$

$$y_i^{n+1} = y_i^n + \eta_i \quad (32)$$

where η_i is a Gaussian distributed random variable with zero mean and variance $2\Delta t/\text{Re}$. The $u=1$ at $y \rightarrow \infty$ and $v=0$ at $y=0$ are automatically satisfied.

The solution to Equation (8) is then the linear combination of the two partial solutions given by equations (28), (29), (31), and (32).

$$x_i^{n+1} = x_i^n + (\Delta t)u_i^n \quad (33)$$

$$y_i^{n+1} = y_i^n + (\Delta t)v_i^n + \eta_i \quad (34)$$

Equations (33) and (34) represent the solution of Equation (8) for a system with no solid boundary. But $u=0$ must be satisfied in the presence of a solid surface. According to Chorin⁶, this is achieved by the vorticity generation at the solid surface.

$\vec{u}_0 = (u_0, v_0)$ is the flow obtained from the solution procedure described above, therefore, it does not satisfy $u=0$ at $y=0$. At the wall, the effect of viscosity will be to create a thin boundary layer adjacent to the wall, the total vorticity in the layer per unit length of the wall is

$$\int_{\text{wall}}^{\text{boundary layer}} \xi dy = u_0 (y=0) \quad (35)$$

One has to create a vortex sheet of strength $u_0 (y=0)$ per unit length of wall. This vortex sheet is then broken up to elements and allowed to participate in the subsequent motion of the fluid according to Equations (33) and (34).

Thus on the wall, points Q_1, \dots, Q_m are designated such that distances $\overline{Q_1 Q_2}, \overline{Q_2 Q_3}, \dots, \overline{Q_{m-1} Q_m}$, equal h . At each point Q_i , the tangential velocity $u_0(Q_i)$ is evaluated using equation (19). Then an original big vortex sheet of strength $2u_0(Q_i)$ is created at Q_i . The random wall scheme requires a large number of vortex sheet elements to converge properly. Before this original vortex sheet is allowed to move out, it is broken into a number of vortex sheets of equal intensity and their total intensity is equal to $2u_0(Q_i)$. Then these group of vortex sheets are allowed to move according to Equations (33) and (34) the next time step.

B. Particle Transport

A fluid stream containing particles flows over a surface, particles are transported and deposited by various mechanisms depending on their sizes and the flow field. As mentioned earlier, the particle transport is

basically by molecular and turbulent diffusion if the particle size is less than 10μ . But simultaneously the momentum of larger particles should be included when they approach the solid surface. According to Fick's Law, the particle flux normal to the flat plate, G , is given by

$$G = -\rho D \frac{\partial m}{\partial y} \quad (36)$$

where ρ is the mixture density, m is the particle mass fraction and D is the binary diffusion coefficient, and it may be written as

$$D = (D_B + D_T) \quad (37)$$

D_B is the Brownian diffusion coefficient due to laminar molecular diffusion. It is given by Einstein formula⁹.

$$D_B = \frac{K_B T}{3\pi\mu d_p} \quad (38)$$

T is the mixture absolute temperature, d_p is the particle diameter, μ is the fluid dynamic viscosity and K_B is Boltzmann constant.

D_T is the turbulent contribution for particle diffusion. Unless the particle is extremely small, D_T is several orders of magnitude greater than D_B . As suggested by Liu and Ilori¹⁰, D_T is

⁹Einstein, A., Theory of Brownian Motion, E. P. Dotton Co.

¹⁰Liu, B.Y.H., and Ilori, T.A., "Aerosol Deposition in Turbulent Pipe Flow," Environmental Science and Technology, 8, 1974.

$$D_T = \epsilon_f + \frac{\rho_p d_p^2 y^2 \tau_w^2}{18\mu(y\sqrt{\rho\tau_w} + 10\mu)^2} \quad (39)$$

ϵ_f is the fluid momentum eddy diffusivity, ρ_p is the particle density, τ_w is shear stress at the surface. The second term is introduced for particle size correction.

Next, the particle transport equation in a boundary layer is described.

Basic assumptions adopted are as follows:

1. The particle mass fraction is small enough so that the fluid properties are unaffected by the presence of the particles.
2. Particles are small such that molecular and turbulent diffusions are the only transport mechanism in the boundary layer.
3. The interior of the particles are included near the solid surface using the free flight theory of Friedlander and Johnstone¹.

The geometry and the system coordinates are shown in Figure 2. The conservation of particles is governed by

$$\frac{\partial m}{\partial t} + u \frac{\partial m}{\partial x} + v \frac{\partial m}{\partial y} = D \frac{\partial^2 m}{\partial y^2} \quad (40)$$

Initial and boundary conditions

$$m = m_\infty, \quad t=0 \quad (41)$$

$$m = m_\infty, \quad y \rightarrow 0, \quad t > 0 \quad (42)$$

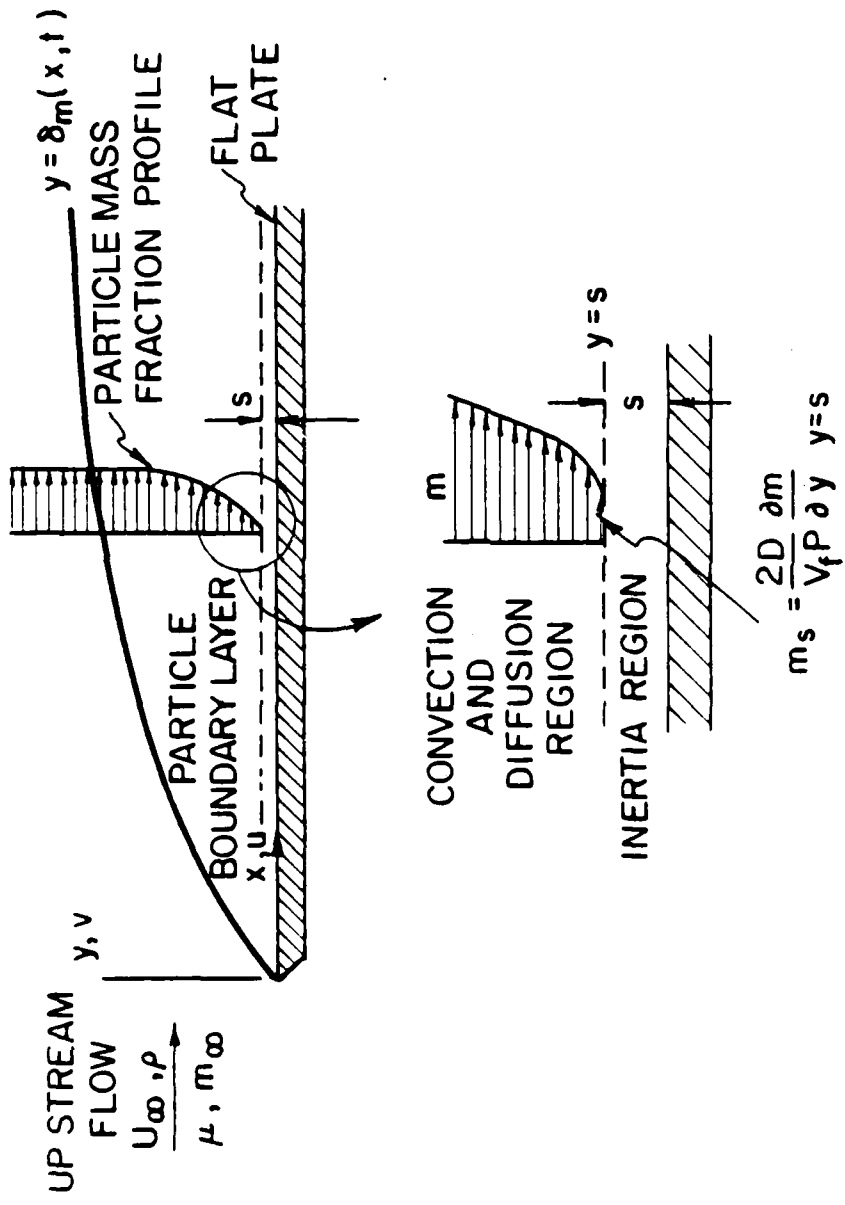


Figure 2. Particle Transport Mechanism at the Boundary

$$m = m_{\infty}, x=0, t>0$$

(43)

The boundary condition at the wall needs some special attention in order to include the particle inertia effects. Because the presence of the wall, the particles behave differently from their diffusion-convection transport in the interior of the boundary layer. According to the theory of Friedlander and Johnstone¹, particles of relative larger diameter coming that close to the wall need only a small impetus to reach the surface. This impetus is the particle inertia. In more detail, particles transport toward the wall occurs by diffusion until they reach the stopping distance from the wall. Particles are considered to complete the final phase of their travel by way of a free flight (inertia coasting) which takes place under the momentum imparted by molecular Brownian motion or turbulent fluctuations. By assuming Stokes flow and taking into account the particle radius, the particle stopping distance may be calculated from the following equation

$$S = \frac{\rho_p d^2 v_s}{18\mu} + \frac{d}{2} \quad (44)$$

where S is the stopping distance and v_s denotes the free flight initial velocity. As Beal³ points out v_s may be determined by summing the Brownian velocity due to molecular motion and root-mean-square normal fluctuation velocity at the stopping distance. Therefore,

$$v_s = \left(\frac{3K_B T}{2 \rho_p d^3} \right)^{1/2} + \frac{S \tau_w}{S \sqrt{\rho \tau_w} + 10\mu} \quad (45)$$

The stopping distance S and initial velocity v_s are solved by iteration from Equations (44) and (45).

The particle flux at the stopping distance ($y=S$) is

$$G_s = \rho D \frac{\partial m}{\partial y} \Big|_{y=s} \quad (46)$$

For simplicity, the particles crossing $y=s$ line are assumed to be transported to the wall at an average velocity v_c which approximately is equal to $v_s/2$. The flow of particles that reach the wall and are captured is then given by

$$G_w = \frac{v_c}{2} P \rho m_s \quad (47)$$

where P is the fraction of the particles which stick on impact. The average velocity is halved because there is equal probability of particles being thrown back toward the main stream. m_s is the mass fraction of particles at the stopping distance. Assuming local equilibrium which was tested by Beal³, then

$$m_s = \frac{2D}{v_c P} \frac{\partial m}{\partial y} \Big|_{y=s} \quad (48)$$

The above is the required boundary condition at $y=S$.

Next, we will non-dimensionalize the transport equation. Let $\bar{u}=u/u_\infty$, $\bar{v}=v/v_\infty$, $\bar{\theta}=m/m_\infty$, $\bar{x}=x/L$, $\bar{y}=y/L$, $\bar{t}=tu_\infty/L$, equation (40) and the auxiliary conditions become

$$\frac{\partial \bar{\theta}}{\partial \bar{t}} + \bar{u} \frac{\partial \bar{\theta}}{\partial \bar{x}} + \bar{v} \frac{\partial \bar{\theta}}{\partial \bar{y}} = \frac{1}{Pe} \frac{\partial^2 \bar{\theta}}{\partial \bar{y}^2}, \quad Pe = Re \cdot Sc \quad (49)$$

$$Sc = \nu/D$$

$$\bar{\theta} = 1, \quad \bar{t} = 0^+ \quad (50)$$

$$\theta = 1, \bar{y} \rightarrow \infty, \bar{t} > 0 \text{ and } \bar{x} = 0, \bar{t} > 0 \quad (51)$$

$$O_s = \text{Tr} \frac{\partial \theta}{\partial y} \Big|_{y=S/L}, \text{Tr} = \frac{2D}{v_c PL} \quad (52)$$

where Tr is a dimensionless number which measures the relative importance of diffusion to inertia transport mechanisms. The bars are dropped from this point on.

Equations (49)-(52) are solved numerically by a finite difference technique. The Strongly Implicit Procedure (SIP) developed by Stone⁷ is employed to solve the transient equation. The SIP has been tested by Lin et al.¹¹ for a complicated problem of transient separated flow over a circular cylinder. They concluded that the SIP results in best accuracy and least amount of computer time compared with other popular methods. An upwind difference is used for the convective term in view of the reverse flow during the unsteady flow motion. A staggered system is considered and it is shown in Figure 3.

The finite difference version of Equation (49) is given as follows,

$$\begin{aligned} & (\theta_{i,j}^{n+1} - \theta_{i,j}^n) + \frac{\Delta t}{\Delta x} \{ \theta_{i,j}^{n+1} [u_{i+1/2,j}, 0] - \theta_{i+1,j}^{n+1} [-u_{i+1/2,j}, 0] - \\ & \theta_{i-1,j}^{n+1} [u_{i-1/2,j}, 0] + \theta_{i,j}^{n+1} [-u_{i-1/2,j}, 0] \} + \frac{\Delta t}{\Delta y} \{ \theta_{i,j}^{n+1} [v_{i,j+1/2}, 0] \\ & - \theta_{i-j+1}^{n+1} [-v_{i,j+1/2}, 0] - \theta_{i,j-1}^{n+1} [v_{i,j-1/2}, 0] + \theta_{i,j}^{n+1} [-v_{i,j-1/2}, 0] \} \\ & = \frac{\Delta t}{\text{Pe}(\Delta y)^2} (\theta_{i,j+1}^{n+1} - 2\theta_{i,j}^{n+1} + \theta_{i,j-1}^{n+1}) \end{aligned} \quad (53)$$

where $[A, B]$ means the greater of A and B.

¹¹ Lin, C.L., Pepper, D.W., and Lee, S.C., "Numerical Methods for Separated Flow Solutions around a Circular Cylinder," AIAA J., 14, 900-906, 1976.

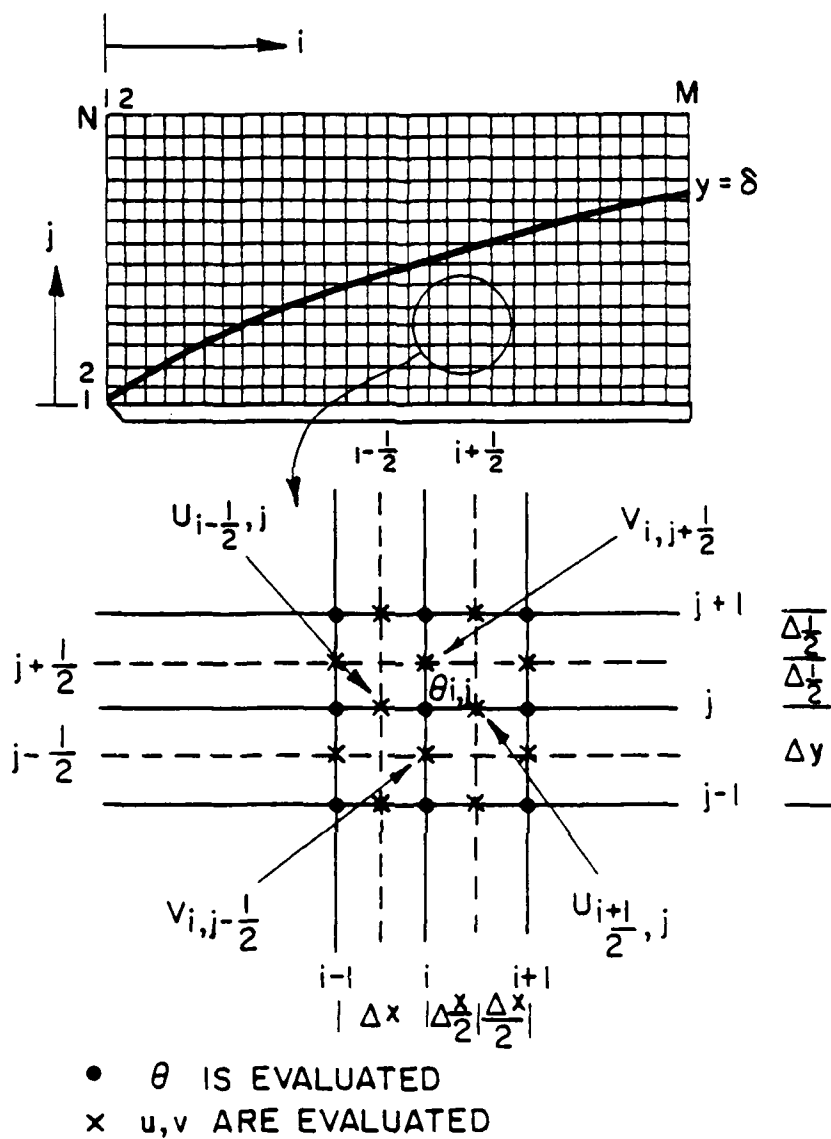


Figure 3. The Grid System for Transport Equation.

In matrix form, Equation (53) becomes,

$$E_{ij} \Theta_{i,j-1}^{n+1} + F_{ij} \Theta_{i-1,j}^{n+1} + G_{ij} \Theta_{ij}^{n+1} + H_{ij} \Theta_{i+1,j}^{n+1} + I_{ij} \Theta_{i,j+1}^{n+1} = J_{ij} \quad (54)$$

$$E_{ij} = [v_{i,j-1/2}, 0] \frac{\Delta t}{\Delta y} - \frac{\Delta t}{Sc(\Delta y)^2} \quad (55)$$

$$F_{ij} = -[u_{i,j-1/2}, 0] \frac{\Delta t}{\Delta x} \quad (56)$$

$$G_{ij} = [1 + ([u_{i+1/2,j}, 0] + [-u_{i-1/2,j}, 0]) \frac{\Delta t}{\Delta x} + ([v_{i,j+1/2}, 0] + [-v_{i,j-1/2}, 0]) \frac{\Delta t}{\Delta y} + \frac{2\Delta t}{Pe(\Delta y)^2}] \quad (57)$$

$$H_{ij} = -[-u_{i+1/2,j}, v] \frac{\Delta t}{\Delta x} \quad (58)$$

$$I_{ij} = -[-v_{i,j+1/2}, 0] \frac{\Delta t}{\Delta y} - \frac{\Delta t}{Pe(\Delta y)^2} \quad (59)$$

$$J_{ij} = Q_{i,j}^n \quad (60)$$

In the above, the subscripts i, j denote the grid point locations and the superscript N denotes the time step number.

The initial and boundary conditions become

$$\Theta_{i,j}^1 = 1 \quad (61)$$

$$\Theta_{i,N} = 1, \quad i=1, \dots, M \quad (62)$$

$$O_{1,j} = 1, j=1, \dots, N \quad (63)$$

$$F_{i1} O_{i-1,1}^{n+1} + \left(G_{i1} - \frac{2\Delta y}{Tr} E_{i1} \right) O_{i,1}^{n+1} + H_{i1} O_{i+1,1}^{n+1} \\ + (I_{i1} + E_{i1}) O_{i,2}^{n+1} = J_{i1}, i=1, \dots, M \quad (64)$$

where $n=1$ corresponds to $t=0^+$, $i=1$ to $x=0$, $i=M$ to $x=1$, $j=1$ to $Y=S/L$ and $j=N$ to $y+\infty$.

The governing equations in matrix form, with five nonzero diagonal elements as the coefficient matrix, may be written as follows

$$[M] \cdot [O^{n+1}] = [O^n] \quad (65)$$

In order to accelerate the solution procedure, matrix $[M]$ is modified as matrix $[M+N]$, which consists of seven nonzero diagonal elements. Equation (64) then becomes

$$[M+N][O^{n+1}]^{m+1} = [O^n] + [N][O^{n+1}]^m \quad (66)$$

in which m is the number of iterations for determining the column matrix $[O]$ at the $(n+1)$ th time step. The modifier matrix $[N]$ had to fulfill the requirement that the coefficient matrix $[M+N]$ can be factored into the product of a lower matrix $[L]$ and an upper matrix $[U]$, each consists of three nonzero diagonal elements in the lower and upper portions. The purpose of this modification is to determine the column matrix $[O^{n+1}]$ by having the difference of the $(m+1)$ th and the (m) th iterations within a prescribed tolerance. If the column matrix $[\Delta O]$ at the $(m+1)$ th iteration is defined as

$$[\Delta\theta^{n+1}]^{m+1} = [\theta^{n+1}]^{m+1} - [\theta^{n+1}]^m \quad (67)$$

then Equation (65) can be written as

$$[M+N] [\Delta\theta^{n+1}]^{m+1} = [\theta^n] - [M][\theta^{n+1}]^m \quad (68)$$

If one uses the lower and upper matrices given the [L] and [U], Equation (67) can be expressed as

$$[L][U][\Delta\theta^{n+1}]^{m+1} = [Q^n] - [M][\theta^{n+1}]^m \quad (69)$$

The use of matrices [L] and [U] accelerates the solution procedure by successive eliminations. Once the column matrix $[\Delta\theta^{n+1}]$ at (m+1) th iteration is equal to or less than the prescribed tolerance, the value of $[\theta^{n+1}]$ at the (m)th iteration become the solution of the new mass fraction of the particle at (n+1)th time step.

A computer code, named PARTRAN, has been developed based on the model presented in the above MATHEMATICAL MODEL section.

VERIFICATION OF THE COMPUTATIONAL SCHEMES

A. Flow Field Calculations

The vortex sheet method was checked with the well known Blasius solution of the steady state flow over a flat plate¹². Due to the nature of the random vortex sheet method, the instantaneous results are expected

¹²Schlichting, H., Boundary Layer Theory, McGraw-Hill, New York, 1960.

to show some fluctuations. Therefore, when comparing with the steady laminar solution of Blasius, only time-averaged velocity profiles are appropriate for comparisons. The test case uses the following input parameters

$$Re = 10^6, \Delta t = 0.2, h = 0.2$$

The instantaneous drag coefficient and the averaged drag coefficient are plotted in Figure 4. The averaging is carried out every twenty time steps.

Figure 5 shows the location of vortex sheets at $t=6.4$. It shows the boundary layer development and the distribution of vorticity.

Figure 6 shows the instantaneous velocity profiles at five different downstream locations at $t=6.4$.

Figure 7 displays the comparison of the three averaged velocity profiles with the Blasius velocity solution.

Based on the comparisons of drag coefficients and velocity profiles, it may be claimed that the vortex sheet method is doing an adequate job. The drag coefficient actually represents the bulk effects. The time averaged drag coefficient goes from $0.429/Re^{1/2}$ for the first twenty time steps, then to $0.642/Re^{1/2}$ the second twenty time steps, and to $0.66/Re^{1/2}$ the third twenty time steps. The Blasius steady state drag coefficient is $0.664/Re^{1/2}$. This tells that the flow will reach steady state in about thirty to forty time steps (6 to 8 dimensionless times). The steady state drag coefficient predicted by the vortex sheet method is almost equal to the exact solution. The variance for the drag coefficient is around $0.03/Re^{1/2}$.

The velocity profile comparisons show the same trend as the drag coefficient. The deviations are all less than 1%.

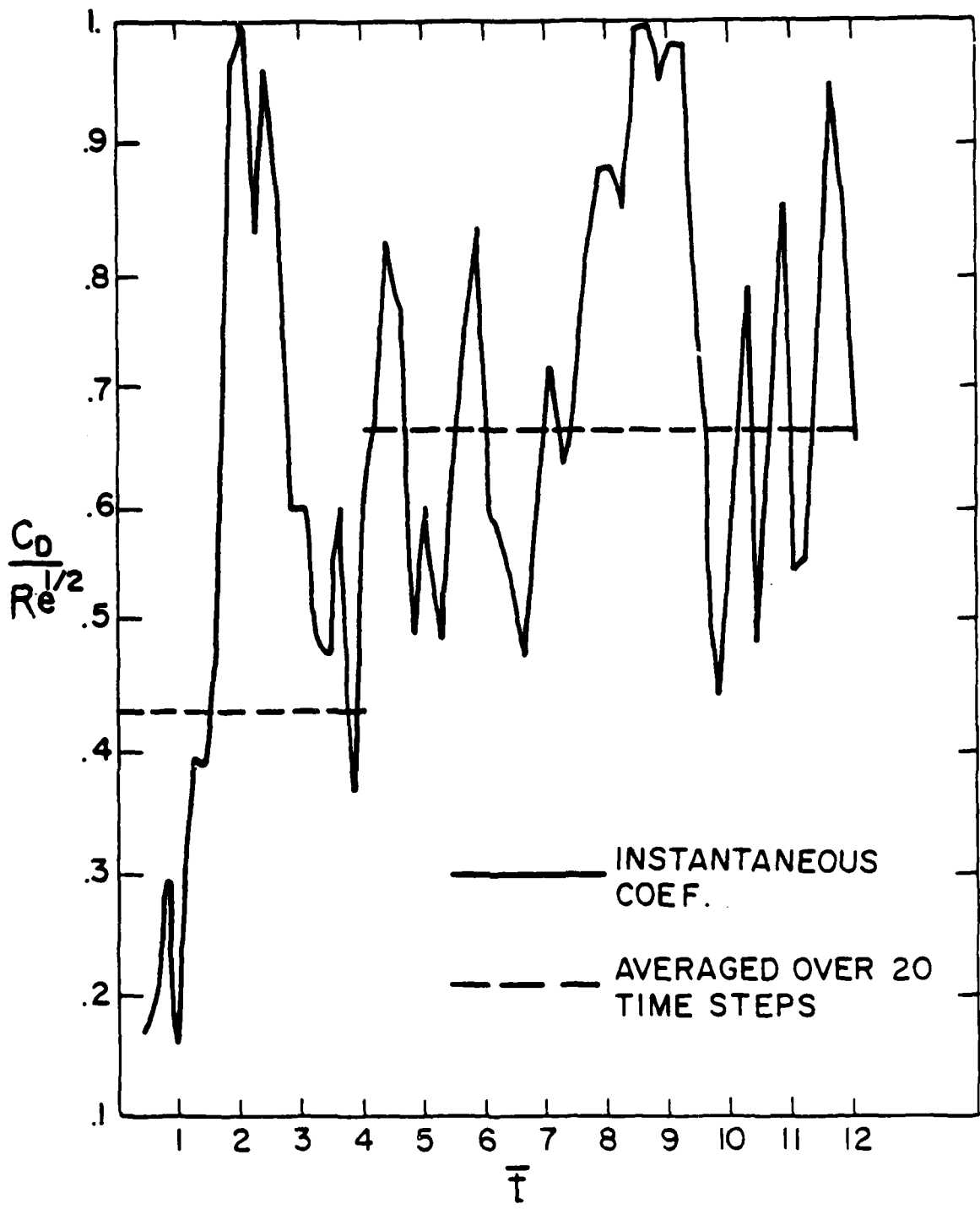


Figure 4. The Drag Coefficient of Impulsive Boundary Layer

Vortex Position

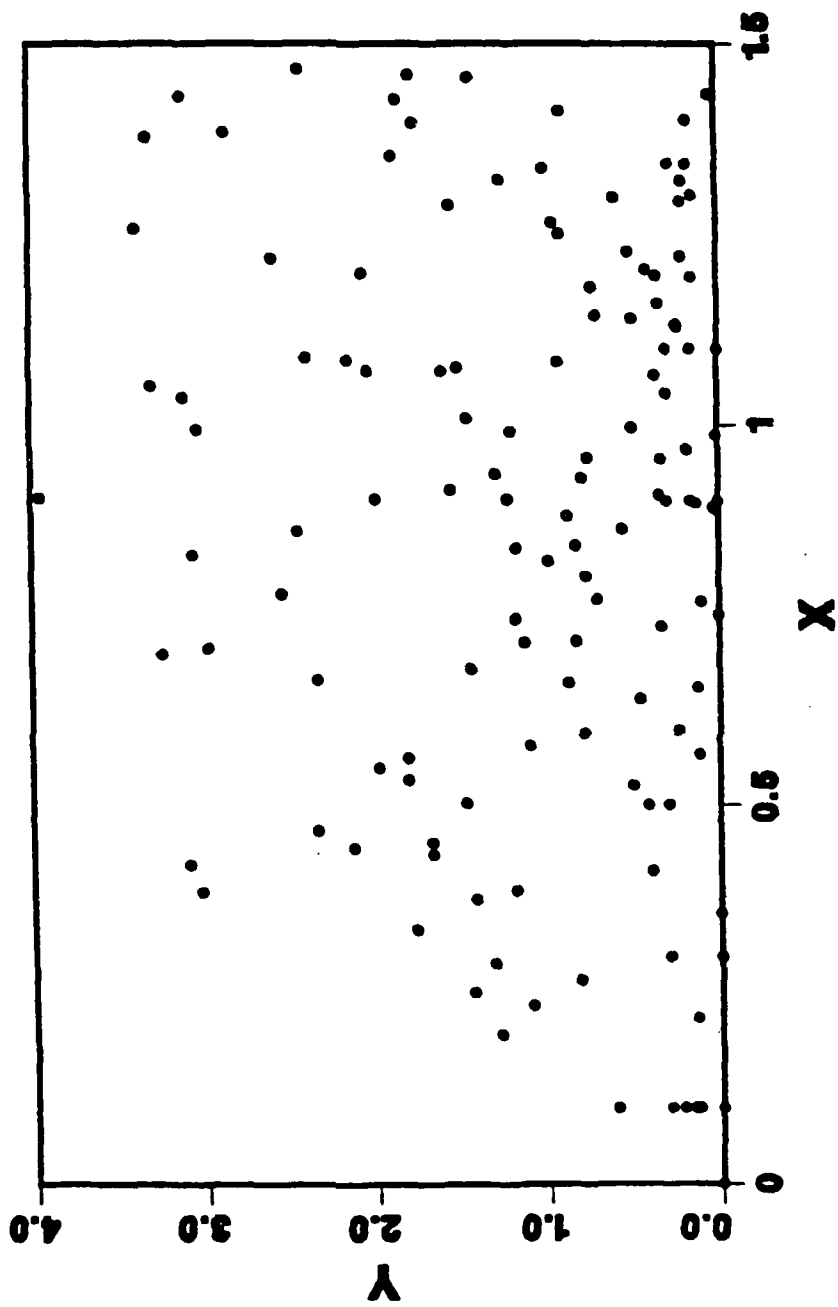


Figure 5. Typical Vortex Sheet Positions in Boundary Layer

Velocity Profiles

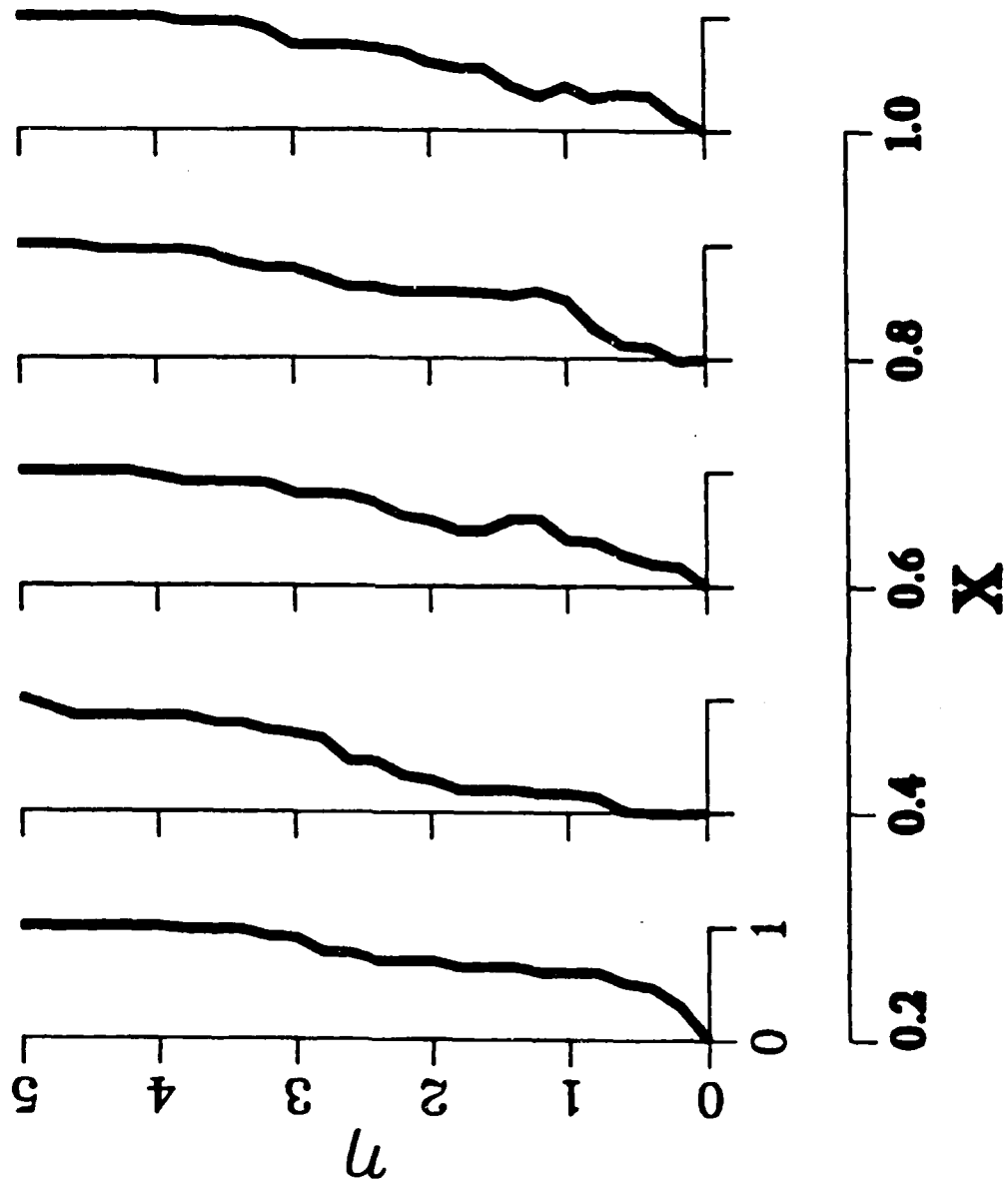


Figure 6. Typical Instantaneous Velocity Profiles

Velocity Profiles

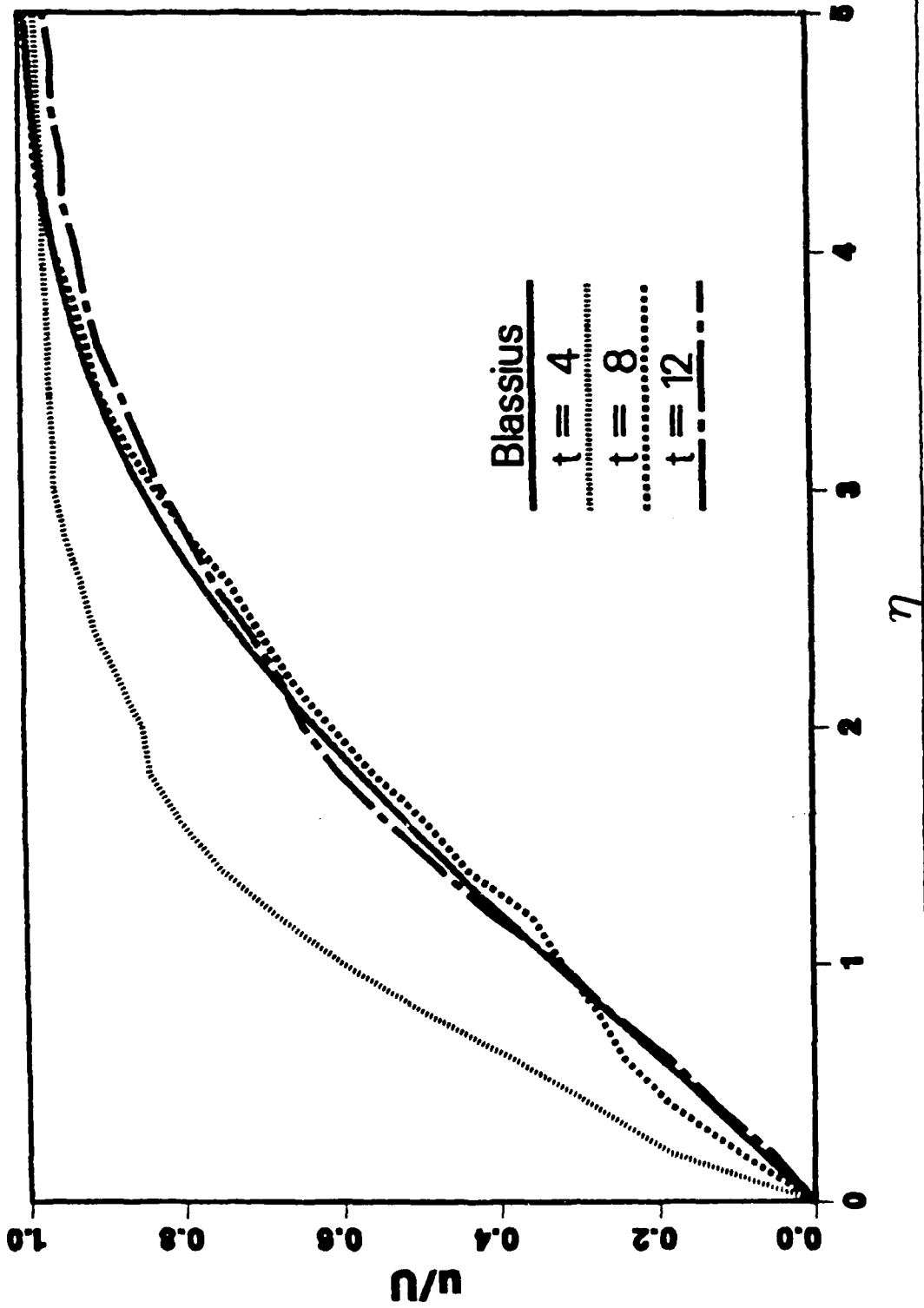


Figure 7. Comparison of Predicted Velocity Profiles with that of the Blasius Solution

B. Particle Transport Computations

B.1 Comparison with Exact Solutions

In order to compare with the exact solution, one of the boundary conditions, Equation (52), has to be changed to the following

$$\theta_s = 0, y = 0 \quad (70)$$

The Tr number is therefore dropped out of the system. Physically it means that wall is a perfect sink for the particle; whenever a particle reaches the surface it will be removed.

With Equation (69) replacing Equation (52), the flow and particle transport equations with auxiliary conditions (8)-(12) and (49)-(52) are reduced to the following for steady state condition

$$u \frac{\partial u}{\partial x} + v \frac{\partial u}{\partial y} = \frac{1}{Re} \frac{\partial^2 u}{\partial y^2}, \quad u=0, v=0, y=0 \quad (71)$$
$$u \rightarrow 1, y \rightarrow \infty$$

$$u \frac{\partial \theta}{\partial x} + v \frac{\partial \theta}{\partial y} = \frac{1}{Pe} \frac{\partial^2 \theta}{\partial y^2}, \quad \theta=0, y=0 \quad (72)$$
$$\theta \rightarrow 1, y \rightarrow \infty$$

Let

$$u = \frac{L}{u_\infty} \frac{\partial \chi}{\partial y}, \quad v = \frac{L}{u_\infty} \frac{\partial \chi}{\partial x} \quad (73)$$

and

$$\lambda = \sqrt{\mu x u_\infty L} f(\eta) \quad (74)$$

$$\eta = y / \sqrt{x/Re} \quad (75)$$

$$f' = u, \quad \theta = \theta(\eta) \quad (76)$$

(70) and (71) become

$$\begin{aligned} f'''' + 1/2 f f'' &= 0 \\ f'(0) &= 0, \quad f'(\infty) \rightarrow 1 \\ f(0) &= 0 \end{aligned} \quad (77)$$

$$\begin{aligned} \theta'' + \frac{Sc}{2} f \theta' &= 0 \\ \theta(0) &= 0 \\ \theta(\infty) &\rightarrow 1 \end{aligned} \quad (78)$$

The exact solution to the above set is given in (12) also,

$$\theta'(0) = 0.332 Sc^{1/3} Re^{1/2} \quad (79)$$

or

$$\left. \frac{\partial \theta(0)}{\partial y} \right|_{\text{average between } 0 \text{ and } x} = 0.664 \sqrt{Re/x} Sc^{1/3} \quad (80)$$

Two cases were selected for comparison. The results are shown in Table 1. Again the solutions from the computer code PARTRAN were averaged over twenty time steps

TABLE 1

CASE	Re	Sc	x	$\partial\theta(0)/\partial y$ by Eq.(79)	$\partial\theta(0)/\partial y$ by PARTRAN
1	10^6	0.7	1	589.57	592.86
2	10^5	1000	1	2099.75	2050.5

Based on Table 1, the good agreement shows that PARTRAN is working correctly.

B.2 Steady State Comparison

This section describes the comparison of the steady state solution of PARTRAN with the solution of Blasius flow coupled with the steady transport equation.

The governing equations are

$$\begin{aligned} f''' + 1/2ff'' &= 0 \\ f'(0) &= 0, f'(\infty) = 1 \\ f(0) &= 0 \end{aligned} \quad (81)$$

$$\begin{aligned} u \frac{\partial \theta}{\partial x} + v \frac{\partial \theta}{\partial y} &= \frac{1}{Pe} \frac{\partial^2 \theta}{\partial y^2} \\ \theta &= 1, y \rightarrow \infty \\ 0 &= Tr \frac{\partial \theta}{\partial y} \text{ at } y = S/L \end{aligned} \quad (82)$$

The computer program BLASIUS was written to solve the set of equations (81) and (82). The Blasius flow is solved by the shooting technique involving fourth-order Runge-Kutta method. The steady transport equation is solved using the same Strongly Implicit Procedure.

The comparison between the results from PARTRAN and those of BLASIUS are shown and discussed in next section - Results and Discussion.

SOLUTION PROCEDURE

Because of the highly fluctuating nature of the vortex sheet flow calculations, proper time-averaging of the velocity is necessary before using it for particle transport calculation. In this analysis, since there is no feedback of the particle on the flow modeling, the complete flow field was calculated and plotted first. By examining the flow fluctuations, piecewise time averaging was performed. The averaging period is corresponding to the fluctuating period of the vortex sheet flow. This smoothed velocity field is then entered in the particle transport calculation using Equation (54). This procedure substantially reduces the numerical errors in the finite difference procedure solving particle transport.

RESULTS AND DISCUSSION

The problem we are investigating corresponds to the physical situation of a suddenly started impulsive flow of a fluid containing particles. This impulsive flow has a uniform velocity of u_∞ before it is over the flat plate. The mass fraction of the particle in the flow before the flat plate is m_∞ . The kinematic viscosity of the fluid is ν and density ρ . The length of the plate is L . The particles in the flow are assumed spherical with diameter d_p and density ρ_p . The binary mass diffusion coefficient between the particle and the fluid is D .

It is noted that even though the geometry chosen here is a simple 2-dimensional cartesian system, the results and trends obtained can be applied to impulsive flow inside a relatively large cylindrical tube. The approximation is valid as long as the boundary layer thickness is small compared with the tube diameter.

The transport equations and their initial and boundary conditions are all represented with dimensionless variables. The results of the calculations are also presented in terms of the dimensionless groups in the system.

After examining the dimensionless governing equations and their auxiliary conditions, three dimensionless groups appear in the system. These are

$$\text{Re} = u_{\infty} L / \nu \quad (83)$$

$$\text{Sc} = \nu / D \quad (84)$$

$$\text{Tr} = 2D / v_f PL \quad (85)$$

Therefore the solutions of the problem may be represented as a function of the above dimensionless groups.

The selection of the ranges of these dimensionless groups is based on practical interests.

The Reynolds number varies between 10^3 and 10^6 . 10^3 is about the lower bound for the boundary layer theory to be valid while 10^6 is in the transition regime. The vortex sheet method has been tested to handle flow up to 10^6 by Chorin⁶, but its ability to deal with the turbulent flow is untested. Theoretically there is no limit to Reynolds number for the vortex sheet model. It should be pointed out that the flows containing particles or pollutants are likely to have earlier transition from laminar to turbulent flows and the transition may last longer than pure flow. The instantaneous flows predicted by the vortex sheet method or other vortex blot method inherently include those fluctuations which may be due to the presence of the particles.

The Schmidt number also has a wide range. For laminar diffusion of particles of the molecular size, e.g., liquid in another liquid, or gas in gas, or gas in liquid, the Sc varies from 0.74 (Oxygen in air) to 1630 (Glycerol liquid in water). When the diffusing particle size gets bigger so does the Sc number. For laminar diffusion of particle of 1μ in air stream using Equation (38), the Sc number is around 10^5 . The Sc number

will be smaller if the turbulent contribution is included [See Equation (37)]. Also the Schmidt number is around 0.9 for turbulent diffusion of molecular size material. Based on the above discussion, the Sc number is set to vary between 0.7 and 10^5 .

The transport number Tr , according to Equation (52), is involved with D , v_f , P , and L . Therefore potentially Tr will have quite a large range. For a 1μ particle in air and laminar flow, the stopping distance is on the order of $10^{-9}m$, the v_f is $10^{-3} m/s$, and Tr is around 10^{-7} with P assumed about unity. Therefore Tr would get larger with small sticking coefficients. Tr is increasing with decreasing particle size and it is usually smaller in turbulent flow than in laminar flow for the same size particle. To cover most cases of practical interest, Tr is given a range of 1 to 10^{-7} .

In the numerical calculation, Δt was set between 0.1 and 0.2, Δx was fixed at 0.025. Δy was determined based on the following equation

$$\Delta y = 0.00005 \times 1000 / \sqrt{Re} \quad (86)$$

The above equation is designed to accommodate the boundary layer size change at different Reynolds numbers because the total number of nodal points is fixed. There are 40 streamwise nodes and 160 vertical nodes.

Based on the stopping distance theory, the vertical (y -direction) nodes should begin at the stopping distance ($y=S$) rather than at the wall. After evaluating the order of magnitude of the stopping distance, it was found that the maximum stopping distance is on the order of $10^{-6}m$ according to Equation (44). Since the Δy is on the order of $10^{-4}m$, it is reasonable to neglect the existence of the stopping distance in the nodal arrangement.

The deposition flux of particles on the plate surface is given by the following dimensional form

$$G_s = \rho D \frac{\partial m}{\partial y} \Big|_{y=s} \quad (87)$$

But we will present the deposition flux in dimensionless form

$$\begin{aligned} \frac{G_s L}{\rho D m^\infty} &= \frac{\partial \theta}{\partial \bar{y}} \Big|_{\bar{y} = S/L} \\ &= - \frac{1}{Tr} \theta_s \\ &= Nu \text{ or } Sh \end{aligned} \quad (88)$$

The dimensionless flux is termed Nusselt number or Sherwood number. In our study, $\bar{Nu}(\bar{t})$ is defined as the average flux at each time step. It is calculated by taking an average over the total $Nu(\bar{t}, \bar{x})$ at those 40 nodal points on the wall.

First we will investigate the effects of different Reynolds numbers on the deposition of particles. The system parameters are kept constant except the Reynolds number Sc is set at 10^3 and Tr at 10^{-6} . The Reynolds number varies from 10^3 to 10^6 . The instantaneous average Nussett number $\bar{Nu}(\bar{t})$, the dimensionless deposition rates, is plotted in Figure 8. As mentioned previously, the random nature of the flow field induces a similar fluctuating particle transport rate. Because all flow fields were generated with the same random number pattern, the random patterns for the deposition rates are more or less identical. The differences among these transport rates are the magnitudes. As expected, higher Reynolds number generates higher deposition rates. From the statistical point of view, more meaningful information for random fluctuations is obtained by time-averaging the instanteneous values. Figure 9 shows the corresponding time-averaged Nussett numbers $\bar{Nu}_{t.a.}(\bar{t})$. The averaging was performed for every five time steps, i.e., one dimensionless time. The curves are fairly smooth and reveal some trends. After very steep drops, they all reach steady state around $\bar{t}=5.6$ dimensionless time. It is noted that in real time, they may not reach steady state at the same time because $\bar{t}=tu_\infty/L$. After some analysis, it was found that the steady state values are well correlated by the following equation

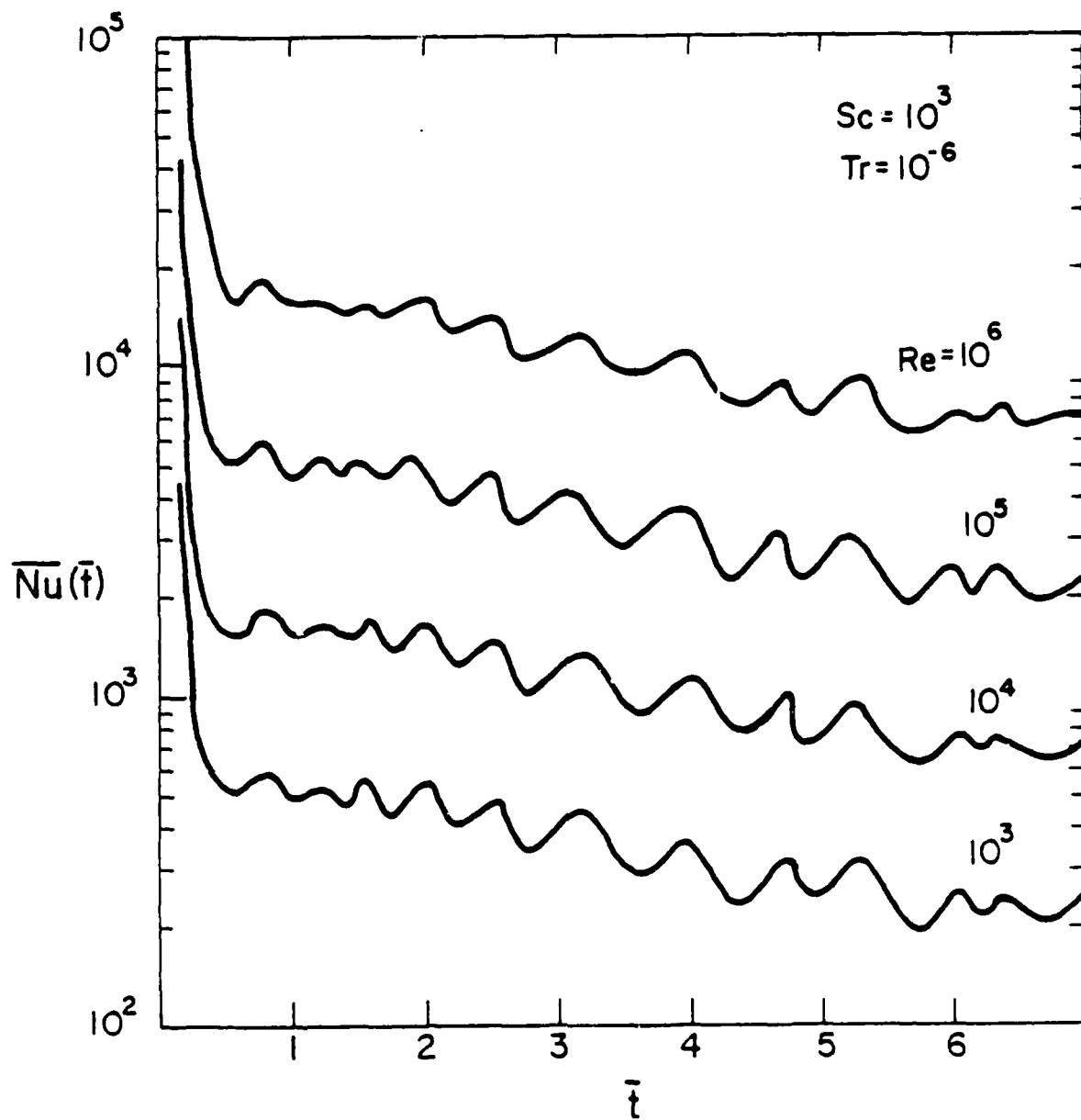


Figure 8. Instantaneous Deposition Rates for Various Reynold Numbers

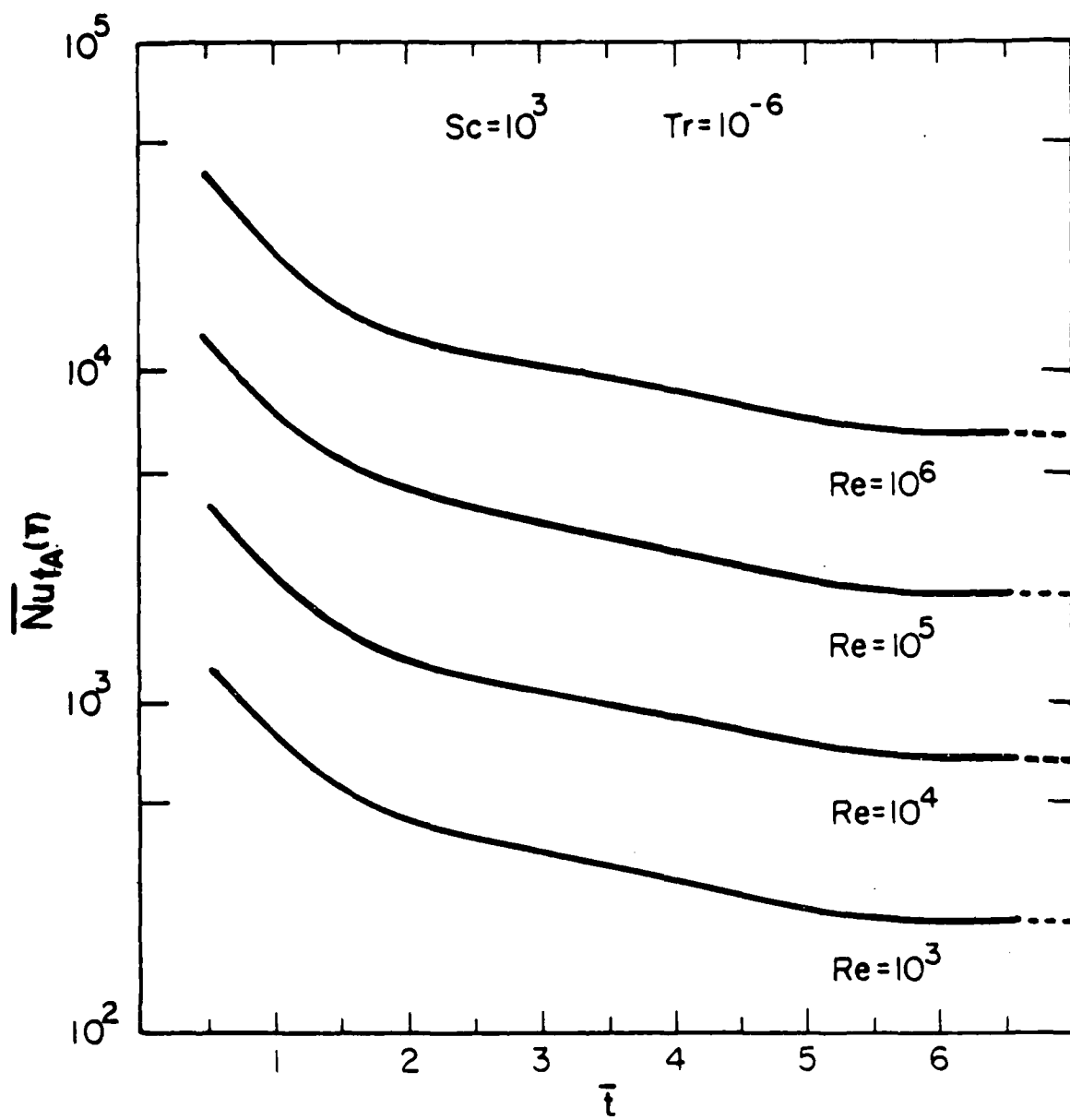


Figure 9. Time-Averaged Deposition Rates for Various Reynold Numbers

$$\frac{(\bar{Nu}_{t.a.})_{\text{steady state}}}{\sqrt{Re}} = 1.7 \quad (89)$$

Another interesting information to examine is the accumulated deposition $W(\bar{t})$, as a function of time, which is plotted in Figure 10. The curves go up quickly in the beginning and then taper off as deposition rates decrease.

A useful formula also was formed for the accumulated depositions,

$$\frac{W(\bar{t}, Re_1)}{\sqrt{Re_1}} = \frac{W(\bar{t}, Re_2)}{\sqrt{Re_2}} \quad (90)$$

The steady state comparisons between the results of PARTRAN and those of BLASIUS are shown in Figure 9. The dashed lines represent the predictions by BLASIUS.

The variation of the Sc on the particle deposition rate is examined in Figure 11, where $Re=10^6$, $Tr=10^{-6}$, and Sc varies from 1 to 10^4 . The transport rates increase with increasing Sc for all the transient cases. Therefore, the same trend extends from the steady state transport to the unsteady transport. In the steady state Equation (79) suggests that \bar{Nu} is proportional to $Sc^{1/3}$. The dashed lines indicate the steady state values of the deposition rates, $\bar{Nu}_{s.s.}$ predicted by the program BLASIUS. It is seen that PARTRAN is doing a good job for Sc of 1, 10, and 10^4 . For intermediate Sc numbers, the steady state transport rates predicted by PARTRAN are much lower than those from BLASIUS. It is believed the results of BLASIUS are correct. The errors of PARTRAN'S predictions are considered primarily due to the truncation errors of the finite difference method. The statistical errors of the flow fields predicated by the vortex sheet method amplify the errors of the finite difference scheme. The fluctuations shown in Figure 8 explain the errors. The predictions of the $\bar{Nu}(t)$ before $\bar{t} < 1.5$ are reasonably good, but the large peak at $\bar{t}=2$ introduces the main truncation errors. It is

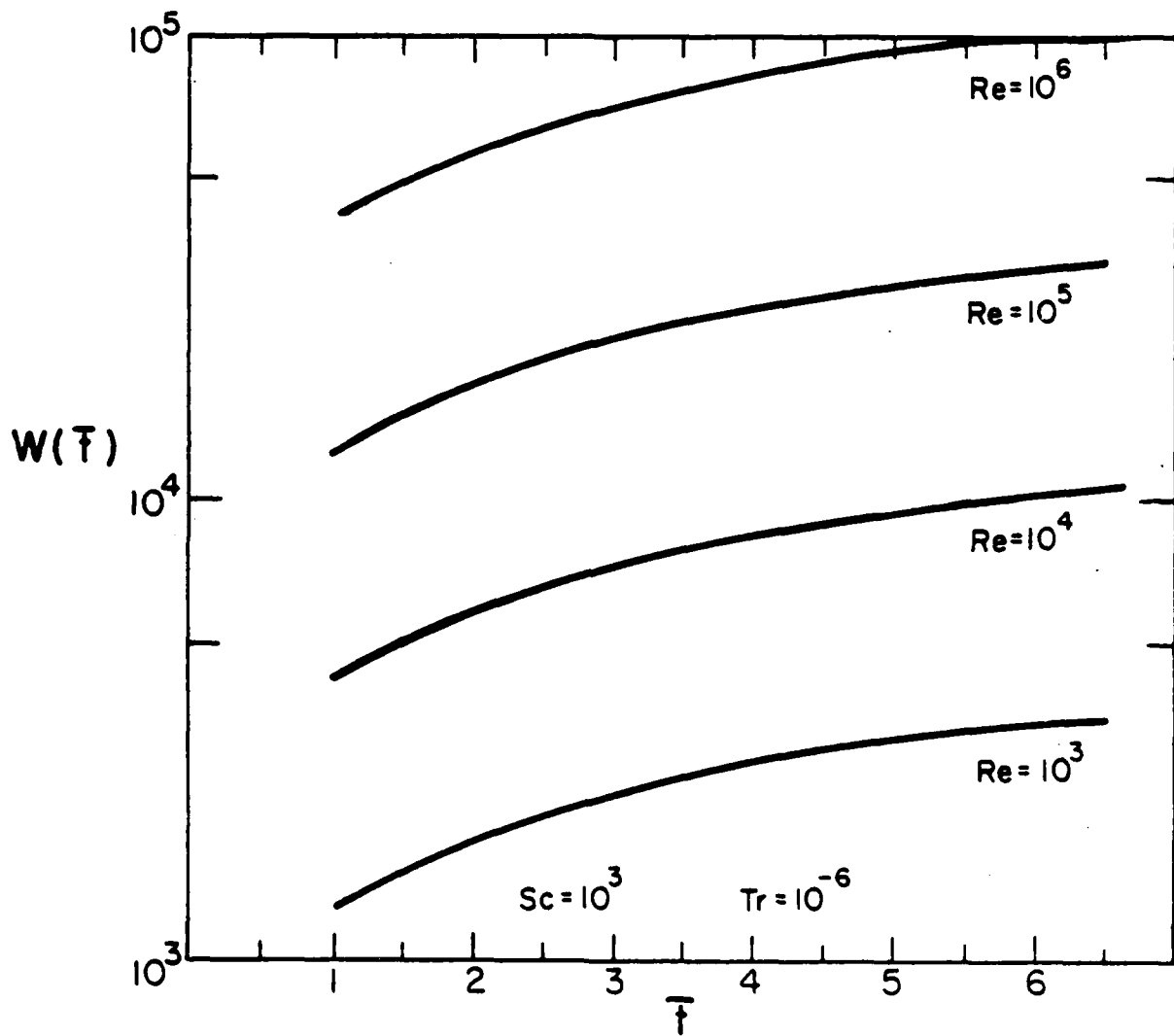


Figure 10. Accumulated Particle Depositions for Various Reynolds Numbers

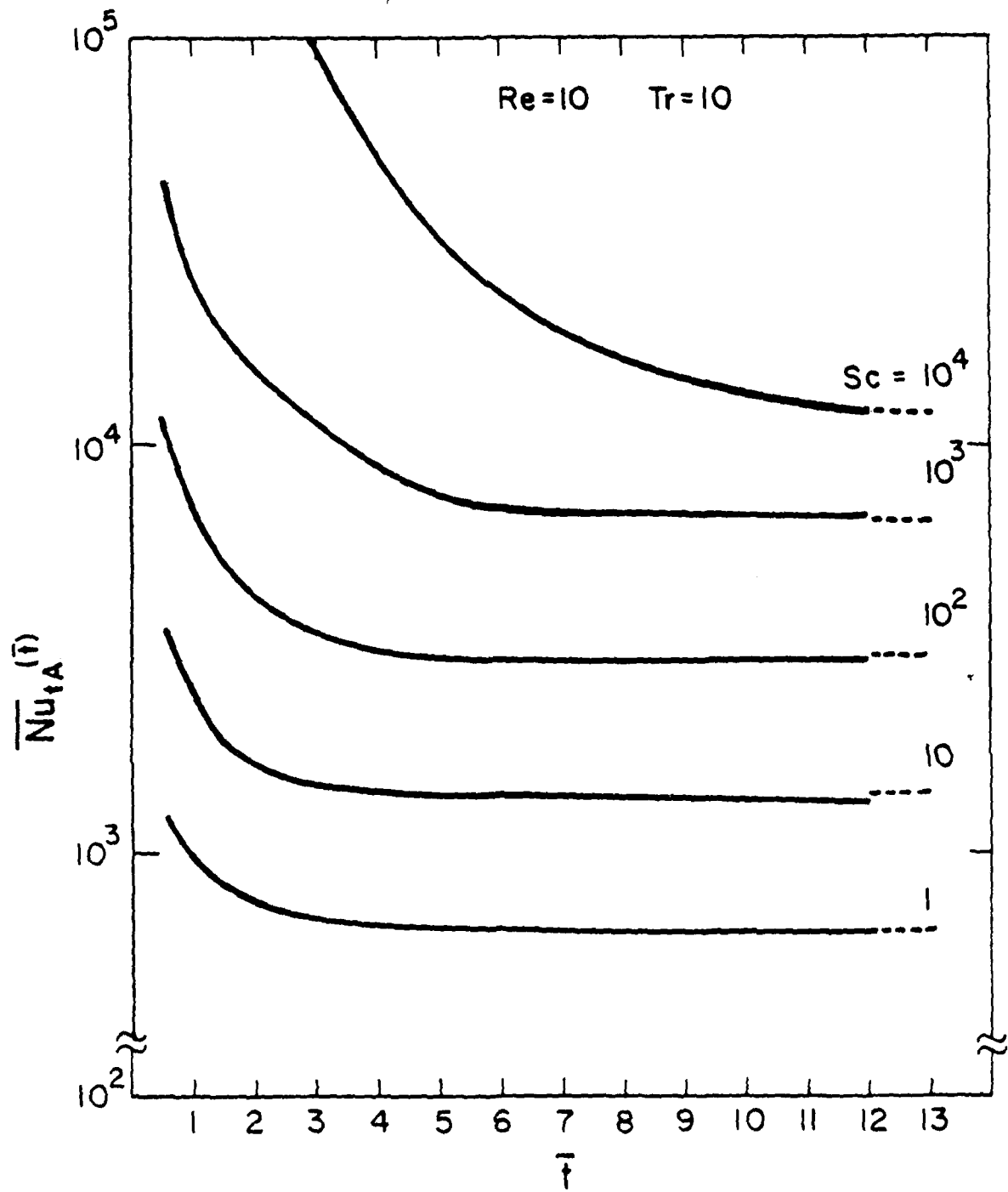


Figure 11. Time-Averaged Deposition Rates for Various Sc Numbers

interesting to note that if the curve were extrapolated after $\bar{t}=2.5$ with the same slope as that before the slope change, the prediction would match very well with the steady state solution predicted by BLASIUS as shown by the chain line.

Figure 12 represents the effects of the Tr number on the time-averaged transport rates. As shown in the figure, the smaller the Tr number, the larger the deposition rates. Since Tr is the ratio of boundary resistance to interior resistance for particle transport, smaller resistance results in higher transport rates, which indicates that the surface resistance is dominant in the process.

The variations of Re, Sc, and Tr on the steady state deposition rates are investigated with the BLASIUS program. Figure 13 examines the Re number variation for several Tr numbers at constant Sc of 10^3 . On a log-log scale the curves are all fairly straight. They more or less fit the relationship of $\bar{Nu}_{s.s.} \propto Re^{1/2}$. The role of Sc number is examined in Figure 14. The straight line portion of the curve for $Tr=10^4$ is represented by $\bar{Nu}_{s.s.} \propto Sc^{1/3}$ quite well. Also $\bar{Nu}_{s.s.}$ increases quickly when Sc is larger than 10^{-3} for $Tr=10^{-3}$. Figure 15 shows the effects of Tr number. Based on the variations of the $\bar{Nu}_{s.s.}$ as a function of Tr, $\bar{Nu}_{s.s.}$ saturates when Tr is smaller than 10^{-5} . This corresponds to the case where the wall is a perfect sink and there is no surface resistance to particle transport and the boundary conditions (52) can be replaced by (69). As Tr gets larger, $\bar{Nu}_{s.s.}$ depends more heavily on its variation.

CONCLUSION

The transport and deposition of fine particles in a boundary layer of impulsive flow over a flat plate have been examined by numerical methods. The transient impulsive flow over a flat plate is solved by a vortex sheet method and the particle transport equation is numerically integrated by the Strongly Implicit Procedure. The transient solutions are preliminary because refinement of the computer program is needed. Some trends and interesting features may be drawn from the results.

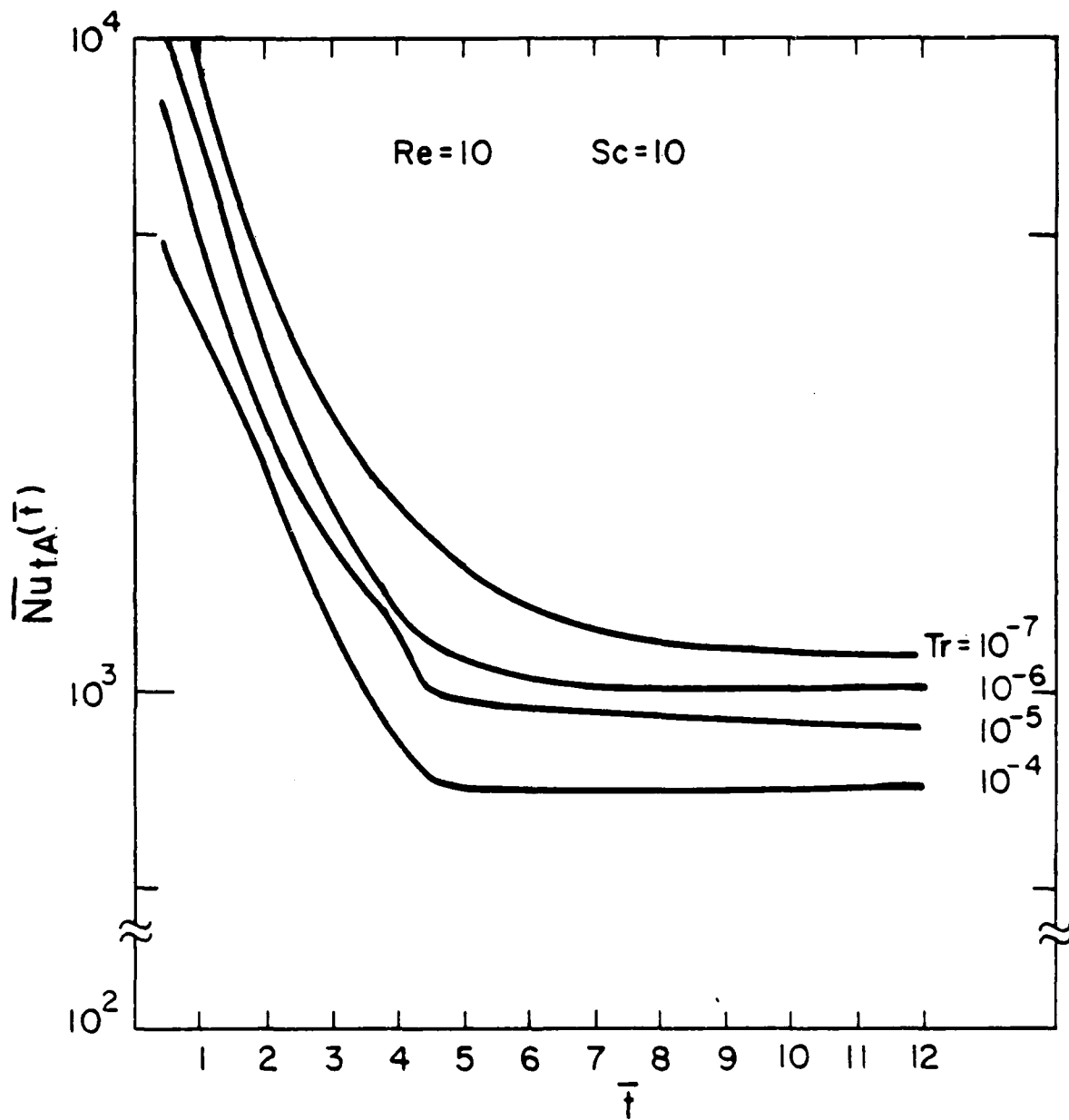


Figure 12. Time-Averaged Deposition Rates for Various Tr Numbers

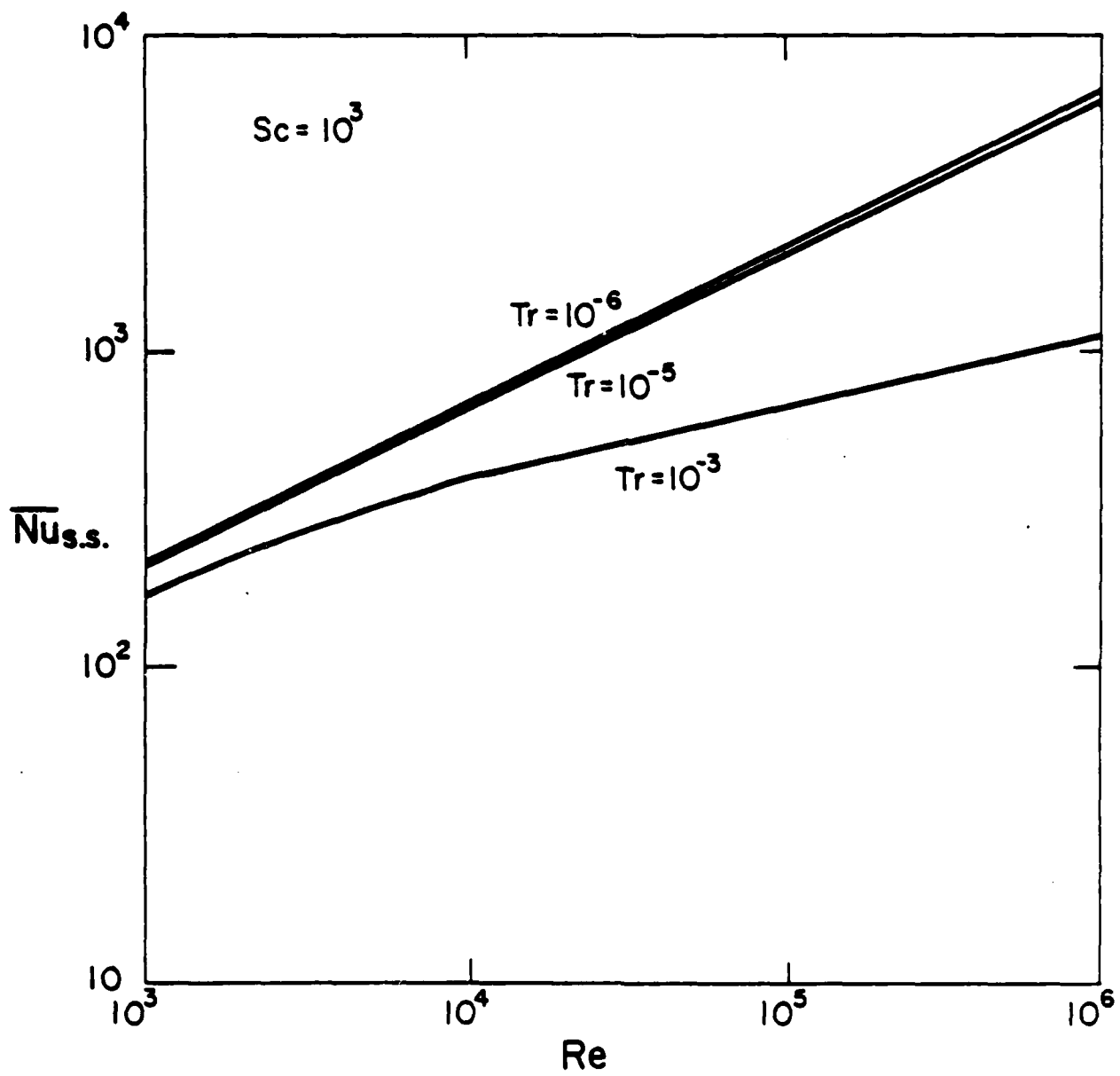


Figure 13. Steady State Deposition Rates as a Function of Reynolds Number

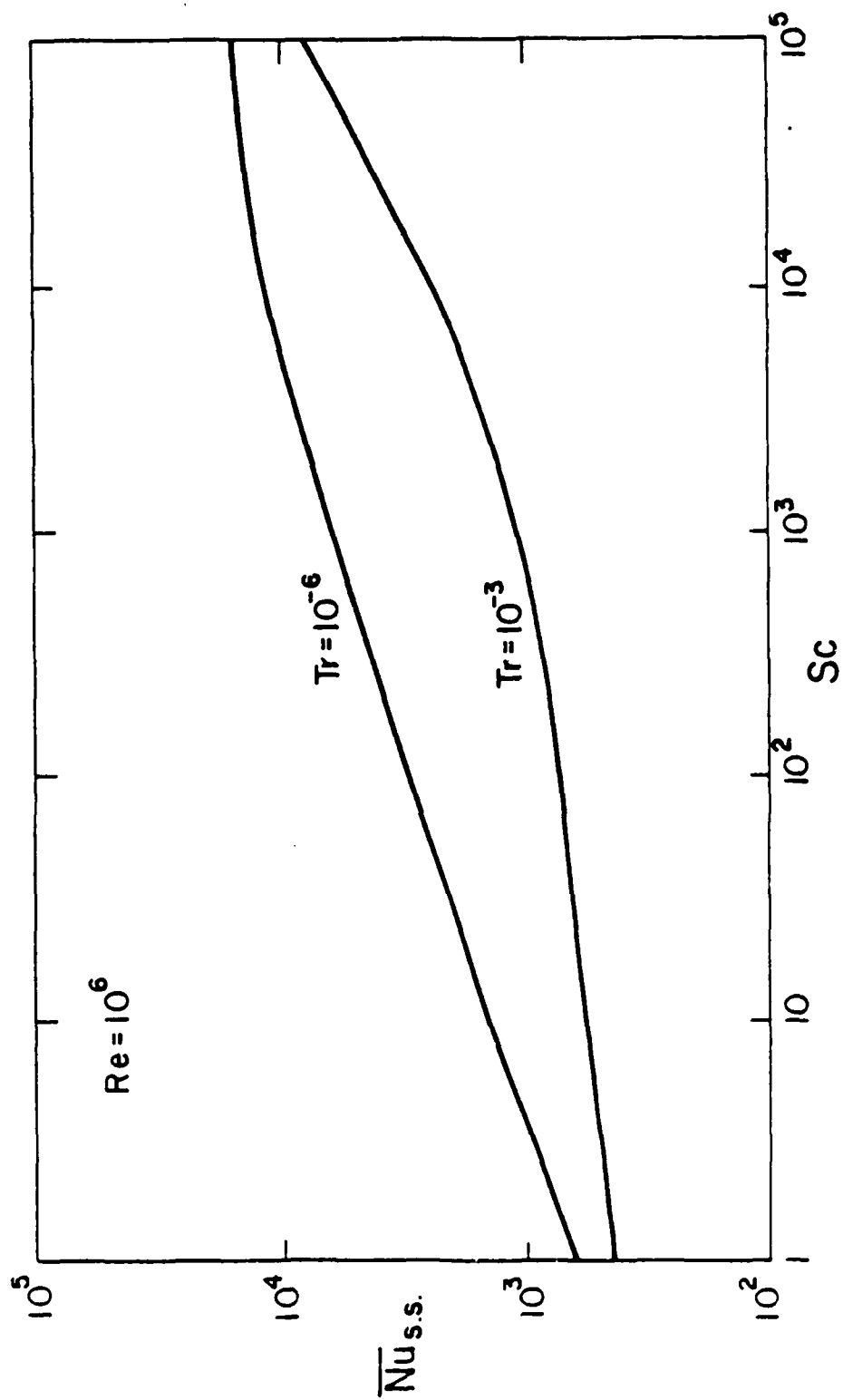


Figure 14. Steady State Deposition Rates as a Function of Schmidt Numbers

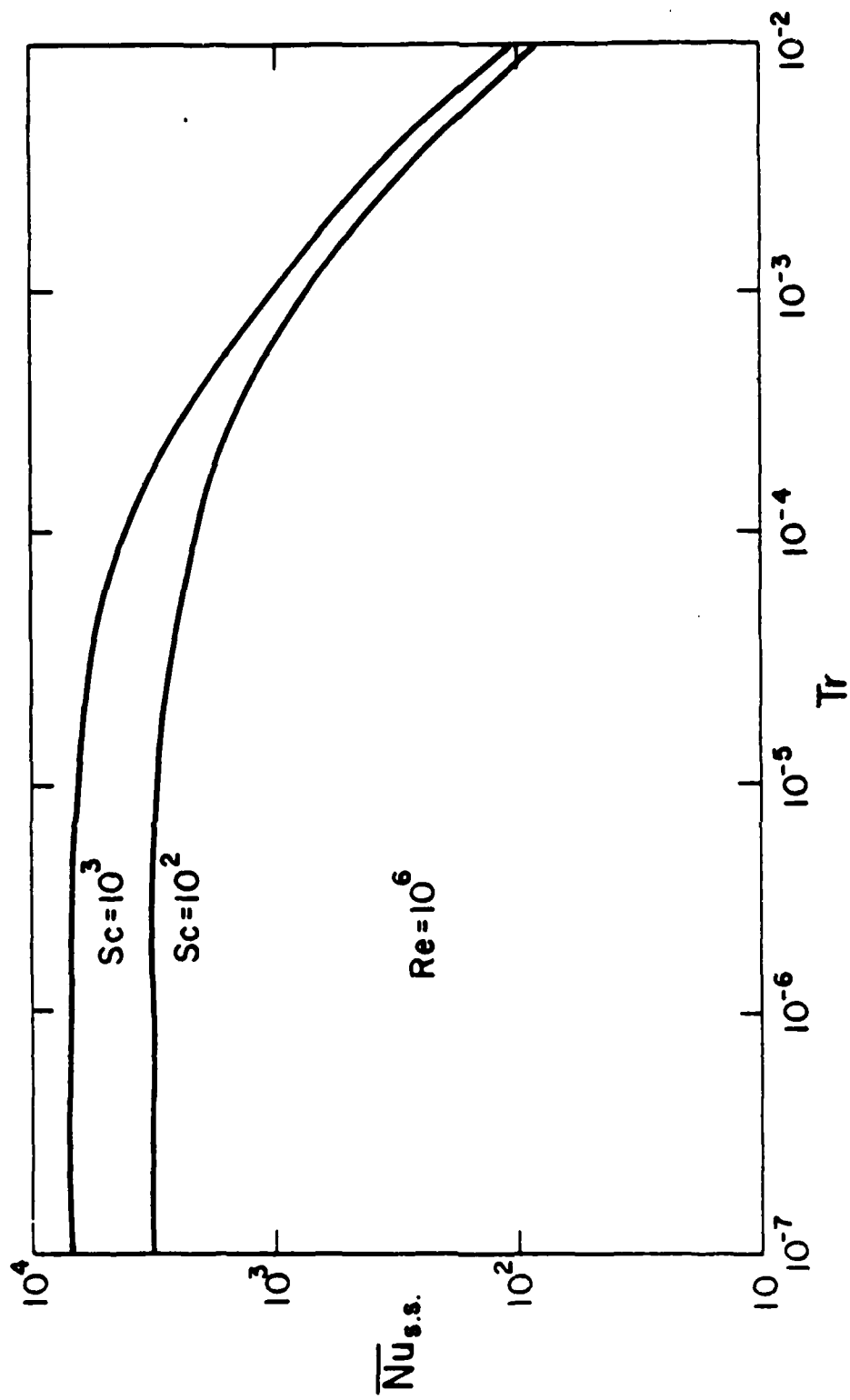


Figure 15. Steady State Deposition Rates as a Function of Transport Numbers

The transport and deposition of the fine particles ($d_p < 10\mu$) are governed by Re , Sc , and Tr . For smaller values of Tr , the dimensionless deposition rates, $\bar{Nu}_{s.s.}$ is proportional to $Re^{1/2}$ and $Sc^{1/3}$. The time to reach steady state seems to be proportional to Sc , inversely proportional to Tr and independent of Re .

The combination of a vortex sheet method for the flow calculations and a finite difference method for the transport equation should be examined more closely. The vortex sheet method is designed for large Reynolds number flow and it is grid free; therefore, the solutions can contain fluctuations due to statistical errors. Those errors may be reduced by averaging the instantaneous solutions. By applying the instantaneous velocity profiles directly into the finite difference transport equation, the statistical errors will amplify the truncation errors. It is thought that the flow solutions by the vortex sheet method should be averaged before coupling them with the transport equation.

RECOMMENDATIONS

1. While the instantaneous flow field predicted by the vortex sheet method represents more or less the actual nature of a high Reynolds number flow, a Lagrange type of approach is more appropriate for investigating the transport of larger particles. The trajectory of each particle is followed by solving the equation of motion for this particle. A large number of sample particles should be introduced, then the overall effects are obtained by performing statistical analysis.

2. The refinement of the PARTRAN computer code should be carried out with an effort first to investigate how to reduce the statistical errors of the random vortex sheet method. Next, investigate the method of reducing the amplification of the statistical method on the truncation errors.

SUMMARY

In many two-phase applications, particle deposition in a boundary layer is strongly dependent upon the flow field and the particle behavior near the wall surface. The boundary layer is a shear flow with different streamwise and vertical characteristics which affect the particle transport and deposition. In transient condition, the developing impulsive boundary layer and the reverse flow will influence both the particle transport and deposition.

The present study is concerned with the transport characteristics of fine particles ($<10\mu$) in an impulsive boundary layer. A random vortex sheet method is used for the flow generation and the transport equation is solved by the Strongly Implicit Procedure of finite difference scheme. The particle depositions are given in terms of the Reynolds number, the Schmidt number and the transport number $T_r = (2D/v_+pL)$. For small values of T_r , the dimensionless deposition rate, $\bar{Nu}_{s.s.}$ is proportional to $Re^{1/2}$ and to $Sc^{1/3}$. The time to reach steady state seems to be proportional to Sc , inversely proportional to T_r and independent on Re . In general, the deposition rates increase with increasing Re and Sc but with decreasing T_r .

The combination of the vortex sheet method and the finite difference method at the current form described in the report does not predict the steady state results for some intermediate Sc . A refinement for the program is needed to reduce the amplification of the statistical errors due to the random vortex method on the truncation errors of the finite difference method in the transport equation.

ACKNOWLEDGEMENT

The author is grateful for the opportunity given by the U.S. Army to participate in the Summer Faculty Research Program.

Special thanks are due to CPT Kurt Fickie, my Contracting Officer's Representative at the Ballistic Research Laboratory. During my visit, CPT Fickie has provided me support and helped define a problem of current

interest to the Army. I also would like to acknowledge the support and interesting discussions with Dr. George Keller.

REFERENCES

1. Friedlander, S.K., and Johnstone, H.F., "Deposition of Suspended Particles from Turbulent Gas Streams," *Industrial and Engineering Chemistry*, 49, 1957.
2. Lin, C.S., Moulton, R.W., and Putman, G.L., "Mass Transfer Between Solid Wall and Fluid Streams," *Industrial and Engineering Chemistry*, 45, 1953.
3. Beal, S.K., "Deposition of Particles in Turbulent Flow on Channel or Pipe Walls," *Nuclear Science and Engineering*, 40, 1970.
4. Menguturk, M. and Sverdrup, E.F., "A Theory for Fine Particle Deposition in Two-Dimensional Boundary Layer Flows and Application to Gas Turbines," *J. of Engineering for Power*, 104, 69-76, 1982.
5. Ganic, E.N. and Rohsenow, W.M., "On the Mechanism of Liquid Drop Deposition in Two-Phase Dispersed Flow," *J. of Heat Transfer*, 101, 228-294, 1979.
6. Chorin, A.J., "Vortex Sheet Approximation of Boundary Layers," *J. of Computational Physics*, 27, 428-442, 1978.
7. Stone, H.L., "Iterative Solution of Implicit Approximations of Multidimensional Partial Differential Equations," *SIAM J. Numerical Analysis*, 5, 530-558, 1968.
8. Chorin, A.J., "Numerical Study of Slightly Viscous Flows," *J. of Fluid Mechanics*, 57, 785-796, 1973.
9. Einstein, A., Theory of Brownian Motion, E. P. Dotton Co.
10. Liu, B.Y.H., and Ilori, T.A., "Aerosol Deposition in Turbulent Pipe Flow," *Environmental Science and Technology*, 8, 1974.
11. Lin, C.L., Pepper, D.W., and Lee, S.C., "Numerical Methods for Separated Flow Solutions around a Circular Cylinder," *AIAA J.*, 14, 900-906, 1976.
12. Schlichting, H., Boundary Layer Theory, McGraw-Hill, New York, 1960.

DISTRIBUTION LIST

<u>No. of Copies</u>	<u>Organization</u>	<u>No. of Copies</u>	<u>Organization</u>
12	Administrator Defense Technical Info Center ATTN: DTIC-FDAC Cameron Station, Bldg 5 Alexandria, VA 22304-6145	5	Project Manager Cannon Artillery Weapons System, ARDC, AMCCOM ATTN: AMCPM-CW, AMCPM-CWV AMCPM-CWS M. Fisette AMCPM-CWA H. Hassmann AMCPM-CWA-S R. DeKleine Dover, NJ 07801-5001
1	Commander USA Concepts Analysis Agency ATTN: D. Hardison 8120 Woodmont Avenue Bethesda, MD 20014-2797		
1	HQDA/DAMA-ZA Washington, DC 20310-2500	2	Project Manager Munitions Production Base Modernization and Expansion ATTN: AMCPM-PBM, A. Siklosi AMCPM-PBM-E, L. Laibson Dover, NJ 07801-5001
1	HQDA, DAMA-CSM, Washington, DC 20310-2500		
1	HQDA/SARDA Washington, DC 20310-2500		
1	C.I.A. OIR/DB/Standard GE47 HQ Washington, D.C. 20505	3	Project Manager Tank Main Armament System ATTN: AMCPM-TMA, K. Russell AMCPM-TMA-105 AMCPM-TMA-120 Dover, NJ 07801-5001
1	Commander US Army War College ATTN: Library-FF229 Carlisle Barracks, PA 17013	1	Commander US Army Watervliet Arsenal ATTN: SARWV-RD, R. Thierry Watervliet, NY 12189-5001
1	US Army Ballistic Missile Defense Systems Command Advanced Technology Center P. O. Box 1500 Huntsville, AL 35807-3801	1	Commander U.S. Army ARDEC ATTN: SMCAR-MSI Dover, NJ 07801-5001
1	Chairman DOD Explosives Safety Board Room 856-C Hoffman Bldg. 1 2461 Eisenhower Avenue Alexandria, VA 22331-9999	1	Commander U.S. Army ARDEC ATTN: SMCAR-TDC Dover, NJ 07801-5001
1	Commander US Army Materiel Command ATTN: AMCPM-GCM-WF 5001 Eisenhower Avenue Alexandria, VA 22333-5001	4	Commander US Army Armament Munitions and Chemical Command ATTN: AMSMC-IMP-L Rock Island, IL 61299-7300
1	Commander US Army Materiel Command ATTN: AMCDRA-ST 5001 Eisenhower Avenue Alexandria, VA 22333-5001	1	HQDA DAMA-ART-M Washington, DC 20310-2500
1	Commander US Army Materiel Command ATTN: AMCDE-DW 5001 Eisenhower Avenue Alexandria, VA 22333-5001	1	Commander US Army AMCCOM ARDEC CCAC ATTN: SMCAR-CCB-TL Benet Weapons Laboratory Watervliet, NY 12189-4050

DISTRIBUTION LIST

<u>No. of Copies</u>	<u>Organization</u>	<u>No. of Copies</u>	<u>Organization</u>
3	Commander US Army ARDEC ATTN: SMCAR-MSI SMCAR-TDC SMCAR-LC LTC N. Barron Dover, NJ 07801-5001	1	Commander US Army Communications - Electronics Command ATTN: AMSEL-ED Fort Monmouth, NJ 07703-5301
7	Commander US Army ARDEC ATTN: SMCAR-LCA A. Beardell D. Downs S. Einstein S. Westley S. Bernstein C. Roller J. Rutkowski Dover, NJ 07801-5001	1	Commander CECOM R&D Technical Library ATTN: AMSEL-M-L (Report Section) B.2700 Fort Monmouth, NJ 07703-5000
3	Commander US Army ARDEC ATTN: SMCAR-LCB-I D. Spring SMCAR-LCE SMCAR-LC-M-E S. Kaplowitz Dover, NJ 07801-5001	1	Commander US Army Harry Diamond Lab. ATTN: DELHD-TA-L 2800 Powder Mill Road Adelphi, MD 20783-1145
4	Commander US Army ARDEC ATTN: SMCAR-LCS SMCAR-LCU-CT E. Barriercs R. Davitt SMCAR-LCU-CV C. Mandala Dover, NJ 07801-5001	1	Commander US Army Missile Command ATTN: AMSMI-RX M.W. Thauer Redstone Arsenal, AL 35898-5249
3	Commander US Army ARDEC ATTN: SMCAR-LCW-A M. Salsbury SMCAR-SCA L. Stiefel B. Brodman Dover, NJ 07801-5001	1	Commander US Army Missile Command Research, Development, and Engineering Center ATTN: AMSMI-RD Redstone Arsenal, AL 35898-5245
1	Commander US Army Aviation Systems Command ATTN: AMSAV-ES 4300 Goodfellow Blvd. St. Louis, MO 63120-1798	1	Commandant US Army Aviation School ATTN: Aviation Agency Fort Rucker, AL 36360
1	Director US Army Aviation Research and Technology Activity Ames Research Center Moffett Field, CA 94035-1099	1	Commander US Army Tank Automotive Command ATTN: AMSTA-TSL Warren, MI 48397-5000
		1	Commander US Army Tank Automotive Command ATTN: AMSTA-CG Warren, MI 48397-5000

DISTRIBUTION LIST

<u>No. of Copies</u>	<u>Organization</u>	<u>No. of Copies</u>	<u>Organization</u>
1	Project Manager Improved TOW Vehicle ATTN: AMCPM-ITV US Army Tank Automotive Command Warren, MI 48397-5000	1	Commander US Army Logistics Mgmt Ctr Defense Logistics Studies Fort Lee, VA 23801
2	Program Manager MI Abrams Tank System ATTN: AMCPM-GMC-SA, T. Dean Warren, MI 48092-2498	1	Commandant US Army Infantry School ATTN: ATSH-CD-CS-OR Fort Benning, GA 31905-5400
1	Project Manager Fighting Vehicle Systems ATTN: AMCPM-FVS Warren, MI 48092-2498	1	Commandant US Army Command and General Staff College Fort Leavenworth, KS 66027
1	President US Army Armor & Engineer Board ATTN: ATZK-AD-S Fort Knox, KY 40121-5200	1	Commandant US Army Special Warfare School ATTN: Rev & Tng Lit Div Fort Bragg, NC 28307
1	Project Manager M-60 Tank Development ATTN: AMCPM-M60TD Warren, MI 48092-2498	3	Commander Radford Army Ammunition Plant ATTN: SMCRA-QA/HI LIB Radford, VA 24141-0298
1	Director US Army TRADOC Systems Analysis Activity ATTN: ATOR-TSL White Sands Missile Range, NM 88002	1	Commander US Army Foreign Science & Technology Center ATTN: AMXST-MC-3 220 Seventh Street, NE Charlottesville, VA 22901-5396
1	Commander US Army Training & Doctrine Command ATTN: ATCD-MA/ MAJ Williams Fort Monroe, VA 23651	2	Commandant US Army Field Artillery Center & School ATTN: ATSF-CO-MW, B. Willis Ft. Sill, OK 73503-5600
2	Commander US Army Materials and Mechanics Research Center ATTN: AMXMR-ATL Tech Library Watertown, MA 02172	1	Commander US Army Development and Employment Agency ATTN: MODE-ORO Fort Lewis, WA 98433-5099
1	Commander US Army Research Office ATTN: Tech Library P. O. Box 12211 Research Triangle Park, NC 27709-2211	1	Office of Naval Research ATTN: Code 473, R. S. Miller 800 N. Quincy Street Arlington, VA 22217-9999
1	Commander US Army Belvoir Research and Development Center ATTN: STRBE-WC Fort Belvoir, VA 22060-5606	3	Commandant US Army Armor School ATTN: ATZK-CD-MS M. Falkovitch Armor Agency Fort Knox, KY 40121-5215

DISTRIBUTION LIST

<u>No. of Copies</u>	<u>Organization</u>	<u>No. of Copies</u>	<u>Organization</u>
2	Commander Naval Sea Systems Command ATTN: SEA 62R SEA 64 Washington, DC 20362-5101	2	Superintendent Naval Postgraduate School Dept. of Mech. Engineering Monterey, CA 93943-5100
1	Commander Naval Air Systems Command ATTN: AIR-954-Tech Lib Washington, DC 20360	1	Program Manager AFOSR Directorate of Aerospace Sciences ATTN: L. H. Caveny Bolling AFB, DC 20332-0001
1	Assistant Secretary of the Navy (R, E, and S) ATTN: R. Reichenbach Room 5E787 Pentagon Bldg. Washington, DC 20350	5	Commander Naval Ordnance Station ATTN: P. L. Stang L Torreyson T. C. Smith D. Brooks Tech Library Indian Head, MD 20640-5000
1	Naval Research Lab Tech Library Washington, DC 20375	1	AFSC/SDOA Andrews AFB, MD 20334
5	Commander Naval Surface Weapons Center ATTN: Code G33, J. L. East W. Burrell J. Johndrow Code G23, D. McClure Code DX-21 Tech Lib Dahlgren, VA 22448-5000	3	AFRPL/DY, Stop 24 ATTN: J. Levine/DYCR R. Corley/DYC D. Williams/DYCC Edwards AFB, CA 93523-5000
2	Comander US Naval Surface Weapons Center ATTN: J. P. Consaga C. Gotzmer Indian Head, MD 20640-5000	1	AFRPL/TSTL (Tech Library) Stop 24 Edwards AFB, CA 93523-5000
4	Commander Naval Surface Weapons Center ATTN: S. Jacobs/Code 240 Code 730 K. Kim/Code R-13 R. Bernecker Silver Spring, MD 20903-5000	1	AFATL/DLYV Eglin AFB, FL 32542-5000
4	Commander Naval Surface Weapons Center ATTN: S. Jacobs/Code 240 Code 730 K. Kim/Code R-13 R. Bernecker Silver Spring, MD 20903-5000	1	AFATL/DLXP Eglin AFB, FL 32542-5000
2	Commanding Officer Naval Underwater Systems Center Energy Conversion Dept. ATTN: CODE 5B331, R. S. Lazar Tech Lib Newport, RI 02840	1	AFATL/DLJE Eglin AFB, FL 32542-5000
2	Commanding Officer Naval Underwater Systems Center Energy Conversion Dept. ATTN: CODE 5B331, R. S. Lazar Tech Lib Newport, RI 02840	1	AFATL/DOIL ATTN: (Tech Info Center) Eglin AFB, FL 32542-5438
4	Commander Naval Weapons Center ATTN: Code 388, R. L. Derr C. F. Price T. Boggs Info. Sci. Div. China Lake, CA 93555-6001	1	NASA/Lyndon B. Johnson Space Center ATTN: NHS-22, Library Section Houston, TX 77054
		1	AFELM, The Rand Corporation ATTN: Library D 1700 Main Street Santa Monica CA 90401-3297

DISTRIBUTION LIST

<u>No. of Copies</u>	<u>Organization</u>	<u>No. of Copies</u>	<u>Organization</u>
1	General Applied Sciences Lab ATTN: J. Erdos Merrick & Stewart Avenues Westbury Long Isl, NY 11590	1	Hercules, Inc. Radford Army Ammunition Plant ATTN: J. Pierce Radford, VA 24141-0299
2	AAI Corporation ATTN: J. Hebert J. Frankle D. Cleveland P. O. Box 6767 Baltimore, MD 21204	1	Honeywell, Inc. - MN64 2200 Defense Systems Division ATTN: C. Hargreaves 6110 Blue Circle Drive Minnetonka MN 55436
1	Aerojet Ordnance Company ATTN: D. Thatcher 2521 Michelle Drive Tustin, CA 92680-7014	1	Lawrence Livermore National Laboratory ATTN: L-355, A. Buckingham M. Finger P. O. Box 808 Livermore, CA 94550-0622
1	Aerojet Solid Propulsion Co. ATTN: P. Micheli Sacramento, CA 95813	1	Lawrence Livermore National Laboratory ATTN: L-324/M. Constantino P. O. Box 808 Livermore, CA 94550-0622
1	Atlantic Research Corporation ATTN: M. K. King 5390 Cheorokee Avenue Alexandria, VA 22312-2302	1	Olin Corporation Badger Army Ammunition Plant ATTN: R. J. Thiede Baraboo, WI 53913
1	AVCO Everett Rsch Lab ATTN: D. Stickler 2385 Revere Beach Parkway Everett, MA 02149-5936	1	Olin Corporation Smokeless Powder Operations ATTN: D. C. Mann P.O. Box 222 St. Marks, FL 32355-0222
2	Calspan Corporation ATTN: C. Morphy P. O. Box 400 Buffalo, NY 14225-0400	1	Paul Gough Associates, Inc. ATTN: P. S. Gough P. O. Box 1614, 1048 South St. Portsmouth, NH 03801-1614
1	General Electric Company Armament Systems Dept. ATTN: M. J. Bulman, Room 1311 128 Lakeside Avenue Burlington, VT 05401-4985	1	Physics International Company ATTN: Library H. Wayne Wampler 2700 Merced Street San Leandro, CA 94577-5602
1	IITRI ATTN: M. J. Klein 10 W. 35th Street Chicago, IL 60616-3799	1	Princeton Combustion Research Lab., Inc. ATTN: M. Summerfield 475 US Highway One Monmouth Junction, NJ 08852-9650
1	Hercules Inc. Allegheny Ballistics Laboratory ATTN: R. B. Miller P. O. Box 210 Cumberland, MD 21501-0210	1	Rockwell International Rocketdyne Division ATTN: BA08 J. E. Flanagan J. Gray 6633 Canoga Avenue Canoga Park, CA 91303-2703
1	Hercules, Inc. Bacchus Works ATTN: K. P. McCarty P. O. Box 98 Magna, UT 84044-0098	2	

DISTRIBUTION LIST

<u>No. of Copies</u>	<u>Organization</u>	<u>No. of Copies</u>	<u>Organization</u>
1	Science Applications, Inc. ATTN: R. B. Edelman 23146 Cumorah Crest Drive Woodland Hills, CA 91364-3710	1	University of Illinois Dept of Mech/Indust Engr ATTN: H. Krier 144 MEB; 1206 N. Green St. Urbana, IL 61801-2978
3	Thiokol Corporation Huntsville Division ATTN: D. Flanigan R. Glick Tech Library Huntsville, AL 35807	1	University of Massachusetts Dept. of Mech. Engineering ATTN: K. Jakus Amherst, MA 01002-0014
2	Thiokol Corporation Elkton Division ATTN: R. Biddle Tech Lib. P. O. Box 241 Elkton, MD 21921-0241	1	University of Minnesota Dept. of Mech. Engineering ATTN: E. Fletcher Minneapolis, MN 55414-3368
2	United Technologies Chemical Systems Division ATTN: R. Brown Tech Library P. O. Box 358 Sunnyvale, CA 94086-9998	1	Case Western Reserve University Division of Aerospace Sciences ATTN: J. Tien Cleveland, OH 44135
1	Veritay Technology, Inc. ATTN: E. Fisher 4845 Millersport Hwy. P. O. Box 305 East Amherst, NY 14051-0305	3	Georgia Institute of Tech School of Aerospace Eng. ATTN: B. T. Zinn E. Price W. C. Strahle Atlanta, GA 30332
1	Universal Propulsion Company ATTN: H. J. McSpadden Black Canyon Stage 1 Box 1140 Phoenix, AZ 85029	1	Institute of Gas Technology ATTN: D. Gidaspow 3424 S. State Street Chicago, IL 60616-3896
1	Battelle Memorial Institute ATTN: Tech Library 505 King Avenue Columbus, OH 43201-2693	1	Johns Hopkins University Applied Physics Laboratory Chemical Propulsion Information Agency ATTN: T. Christian Johns Hopkins Road Laurel, MD 20707-0690
1	Brigham Young University Dept. of Chemical Engineering ATTN: M. Beckstead Provo, UT 84601	1	Massachusetts Institute of Technology Dept of Mechanical Engineering ATTN: T. Toong 77 Massachusetts Avenue Cambridge, MA 02139-4307
1	California Institute of Tech 204 Karman Lab Main Stop 301-46 ATTN: F. E. C. Culick 1201 E. California Street Pasadena, CA 91109	1	G. M. Faeth Pennsylvania State University Applied Research Laboratory University Park, PA 16802-7501
1	California Institute of Tech Jet Propulsion Laboratory ATTN: L. D. Strand 4800 Oak Grove Drive Pasadena, CA 91109-8099	1	Pennsylvania State University Dept. of Mech. Engineering ATTN: K. Kuo University Park, PA 16802-7501

DISTRIBUTION LIST

<u>No. of Copies</u>	<u>Organization</u>	<u>No. of Copies</u>	<u>Organization</u>
1	Purdue University School of Mechanical Engineering ATTN: J. R. Osborn TSPC Chaffee Hall West Lafayette, IN 47907-1199	Cdr, USATECOM ATTN: AMSTE-SI-F AMSTE-CM-F, L. Nealley	
1	SRI International Propulsion Sciences Division ATTN: Tech Library 333 Ravenswood Avenue Menlo Park, CA 94025-3493	Cdr, CSTA ATTN: STECS-AS-H, R. Hendricksen	
1	Rensselaer Polytechnic Inst. Department of Mathematics Troy, NY 12181	Cdr, CRDC, AMCCOM ATTN: SMCCR-RSP-A SMCCR-MU SMCCR-SPS-IL	
2	Director Los Alamos Scientific Lab ATTN: T3, D. Butler M. Division, B. Craig P. O. Box 1663 Los Alamos, NM 87544		
1	Stevens Institute of Technology Davidson Laboratory ATTN: R. McAlevy, III Castle Point Station Hoboken, NJ 07030-5907		
1	Rutgers University Dept. of Mechanical and Aerospace Engineering ATTN: S. Temkin University Heights Campus New Brunswick, NJ 08903		
1	University of Southern California Mechanical Engineering Dept. ATTN: OHE200, M. Gerstein Los Angeles, CA 90089-5199		
2	University of Utah Dept. of Chemical Engineering ATTN: A. Baer G. Flandro Salt Lake City, UT 84112-1194		
1	Washington State University Dept. of Mech. Engineering ATTN: C. T. Crowe Pullman, WA 99163-5201		

Aberdeen Proving Ground

Dir, USAMSAA
ATTN: AMXSY-D
AMXSY-MP, H. Cohen

USER EVALUATION SHEET/CHANGE OF ADDRESS

This Laboratory undertakes a continuing effort to improve the quality of the reports it publishes. Your comments/answers to the items/questions below will aid us in our efforts.

1. BRL Report Number _____ Date of Report _____

2. Date Report Received _____

3. Does this report satisfy a need? (Comment on purpose, related project, or other area of interest for which the report will be used.) _____

4. How specifically, is the report being used? (Information source, design data, procedure, source of ideas, etc.) _____

5. Has the information in this report led to any quantitative savings as far as man-hours or dollars saved, operating costs avoided or efficiencies achieved, etc? If so, please elaborate. _____

6. General Comments. What do you think should be changed to improve future reports? (Indicate changes to organization, technical content, format, etc.) _____

CURRENT ADDRESS
Name _____
Organization _____
Address _____
City, State, Zip _____

7. If indicating a Change of Address or Address Correction, please provide the New or Correct Address in Block 6 above and the Old or Incorrect address below.

OLD ADDRESS
Name _____
Organization _____
Address _____
City, State, Zip _____

(Remove this sheet, fold as indicated, staple or tape closed, and mail.)

FOLD HERE

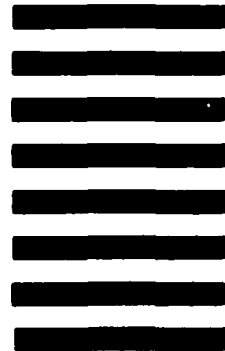
Director
US Army Ballistic Research Laboratory
ATTN: DRXBR-OD-ST
Aberdeen Proving Ground, MD 21005-5066



NO POSTAGE
NECESSARY
IF MAILED
IN THE
UNITED STATES

OFFICIAL BUSINESS
PENALTY FOR PRIVATE USE, \$300

BUSINESS REPLY MAIL
FIRST CLASS PERMIT NO 12062 WASHINGTON, DC
POSTAGE WILL BE PAID BY DEPARTMENT OF THE ARMY



Director
US Army Ballistic Research Laboratory
ATTN: DRXBR-OD-ST
Aberdeen Proving Ground, MD 21005-9989

FOLD HERE

END

DATE

FILMED

5-88

DTIC